Accepted Manuscript

Inhibition of trypanosome alternative oxidase without its N-terminal mitochondrial targeting signal (ΔMTS-TAO) by cationic and non-cationic 4-hydroxybenzoate and 4-alkoxybenzaldehyde derivatives active against *T. brucei* and *T. congolense*

Godwin U. Ebiloma, Teresa Díaz Ayuga, Emmanuel O. Balogun, Lucía Abad Gil, Anne Donachie, Marcel Kaiser, Tomás Herraiz, Daniel K. Inaoka, Tomoo Shiba, Shigeharu Harada, Kiyoshi Kita, Harry P. de Koning, Christophe Dardonville

PII: S0223-5234(18)30212-5

DOI: 10.1016/j.ejmech.2018.02.075

Reference: EJMECH 10252

To appear in: *European Journal of Medicinal Chemistry*

Received Date: 30 November 2017

Revised Date: 22 February 2018

Accepted Date: 23 February 2018

Please cite this article as: G.U. Ebiloma, Teresa.Dí. Ayuga, E.O. Balogun, Lucí.Abad. Gil, A. Donachie, M. Kaiser, Tomá. Herraiz, D.K. Inaoka, T. Shiba, S. Harada, K. Kita, H.P. de Koning, C. Dardonville, Inhibition of trypanosome alternative oxidase without its N-terminal mitochondrial targeting signal (ΔMTS-TAO) by cationic and non-cationic 4-hydroxybenzoate and 4-alkoxybenzaldehyde derivatives active against *T. brucei* and *T. congolense*, *European Journal of Medicinal Chemistry* (2018), doi: 10.1016/j.ejmech.2018.02.075.

Graphical abstract

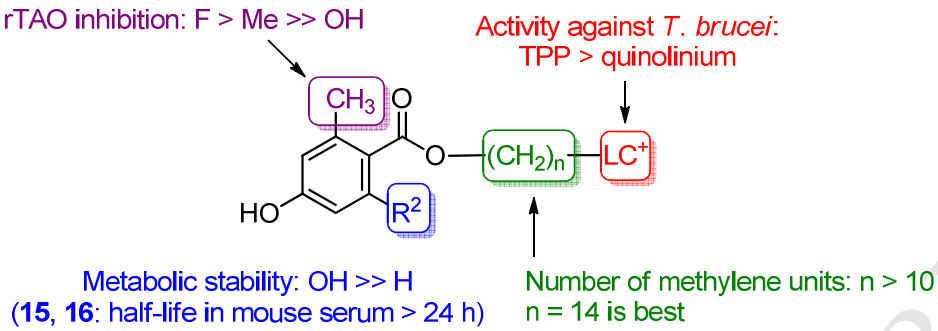

Eur. J. Med. Chem.

Inhibition of Trypanosome Alternative Oxidase without its N-Terminal Mitochondrial Targeting Signal (ΔMTS-TAO) by Cationic and Non-cationic 4-Hydroxybenzoate and 4-Alkoxybenzaldehyde Derivatives Active against *T. brucei* and *T. congolense*

Godwin U. Ebiloma[a,b§], Teresa Díaz Ayuga[c§], Emmanuel O. Balogun[d,e], Lucía Abad Gil[c], Anne Donachie[a], Marcel Kaiser[f], Tomás Herraiz[g], Daniel K. Inaoka[d,h] , Tomoo Shiba[i], Shigeharu Harada[i], Kiyoshi Kita[d,h], Harry P. de Koning[a*], Christophe Dardonville[c*]

[a] Institute of Infection, Immunity and Inflammation, College of Medical, Veterinary and Life Sciences, University of Glasgow, Glasgow, United Kingdom.

[b] Department of Biochemistry, Kogi State University, Anyigba, Nigeria

[c] Instituto de Química Médica, IQM–CSIC, Juan de la Cierva 3, E–28006 Madrid, Spain.

[d] Department of Biomedical Chemistry, Graduate School of Medicine, The University of Tokyo, Japan.

[e] Department of Biochemistry, Ahmadu Bello University, Zaria 2222, Nigeria

[f] Swiss Tropical and Public Health Institute, Socinstrasse, 57, CH-4002 Basel, Switzerland.

[g] Instituto de Ciencia y Tecnología de Alimentos y Nutrición, ICTAN–CSIC, Juan de la Cierva 3, E–28006 Madrid, Spain.

[h] School of Tropical Medicine and Global Health, Nagasaki University, Nagasaki, 852-8523, Japan

[i] Department of Applied Biology, Kyoto Institute of Technology, Kyoto 606-8585, Japan

[§] These authors contributed equally.

ABSTRACT

African trypanosomiasis is a neglected parasitic disease that is still of great public health relevance, and a severe impediment to agriculture in endemic areas. The pathogens possess certain unique metabolic features that can be exploited for the development of new drugs. Notably, they rely on an essential, mitochondrially-localized enzyme, Trypanosome Alternative Oxidase (TAO) for their energy metabolism, which is absent in the mammalian hosts and therefore an attractive target for the design of safe drugs. In this study, we cloned, expressed and purified the physiologically relevant form of TAO, which lacks the N-terminal 25 amino acid mitochondrial targeting sequence (ΔMTS-TAO). A new class of 32 cationic and non-cationic 4-hydroxybenzoate and 4-alkoxybenzaldehyde inhibitors was designed and synthesized, enabling the first structure-activity relationship studies on ΔMTS-TAO. Remarkably, we obtained compounds with enzyme inhibition values (IC_{50}) as low as 2 nM, which were efficacious against wild type and multidrug-resistant strains of *T. brucei* and *T. congolense*. The inhibitors **13**, **15**, **16**, **19**, and **30**, designed with a mitochondrion-targeting lipophilic cation tail, displayed trypanocidal potencies comparable to the reference drugs pentamidine and diminazene, and showed no cross-resistance with the critical diamidine and melaminophenyl arsenical classes of trypanocides. The cationic inhibitors **15**, **16**, **19**, **20**, and **30** were also much more selective (900 - 344,000) over human cells than the non-targeted neutral derivatives (selectivity >8-fold). A preliminary *in vivo* study showed that modest doses of **15** and **16** reduced parasitemia of mice infected with *T. b. rhodesiense* (STIB900). These compounds represent a promising new class of potent and selective hits against African trypanosomes.

Keywords: SHAM, triphenylphosphonium salt (TPP), quinolinium salt, lipophilic cation, trypanosomiasis, trypanocide, mitochondrial targeting, parasite respiration, trypanosome alternative oxidase (TAO), *Trypanosoma brucei*, *T. b. rhodesiense*, *T. congolense*

1. Introduction

Alternative oxidases (AOXs), which are found across a broad range of organisms, including plants, nematodes, algae, yeast and certain disease–causing microorganisms including *Trypanosoma spp.*, are mitochondrial, cyanide–insensitive, membrane-bound proteins that catalyse the oxidation of ubiquinol and the four-electron reduction of oxygen to water [1]. In *T. brucei*, a parasite that causes African trypanosomiasis in humans (sleeping sickness) [2] and in livestock (nagana) [3] throughout sub-Saharan Africa, the trypanosome alternative oxidase (TAO) is essential for the respiration of bloodstream form (BSF) parasites. In effect, in BSF trypanosomes, TAO is the sole terminal oxidase enzyme to re-oxidize the NADH that accumulates during glycolysis, and, as TAO has no counterpart in mammalian cells and is conserved among *T. brucei* subspecies [4], it has been validated as a promising target for the chemotherapy of African trypanosomiasis [5-7].

TAO is a cyanide-resistant and cytochrome-independent ubiquinol oxidase, formerly known as glycerol-3-phosphate oxidase, which is sensitive to the specific inhibitors salicylhydroxamic acid (SHAM) and ascofuranone (AF) [8-11]. Recently, we showed that dihydroxybenzoates and salicylhydroxamates could be efficiently targeted to the *T. brucei* mitochondrial matrix, by coupling them to a lipophilic cation [12]. A preliminary assessment of their antitrypanosomal activity found that some of these compounds appeared to inhibit TAO, which inspired the current strategy of synthesizing a small library of analogs optimized for (a) mitochondrial import and (b) TAO inhibition. As such, a series of 4-Hydroxybenzoate and 4-Alkoxybenzaldehyde derivatives was attached to triphenylphosphonium (TPP) and to quinolinium lipophilic cations, through linkers of variable length that would allow optimal engagement with the TAO binding pocket.

Another issue we addressed for the first time is that previous efforts to screen for, and optimize TAO inhibitors have used a non-physiological version of recombinant TAO that retains the N-terminal Mitochondrial Targeting Sequence (MTS) [13], despite its relatively poor stability and solubility, and its low yield [14]. The AOX gene of *T. brucei* contains 990 nucleotides, encoding the 330 amino acids full length protein, which includes the MTS. This sequence was predicted to be 25 amino acids long, using the computer program MITOPROT (http://www.expasy.org/tools/). As the MTS is cleaved off after transportation of the protein into the mitochondrion, physiologically functional and relevant form of TAO is lacking the MTS sequence [15].

Therefore, in the present study, we report for the first time the production of recombinant TAO enzyme in its more active, physiological state without the N-terminal MTS sequence (ΔMTS-TAO). We also report the novel use of a SUMO expression system to optimize the production of this protein. The ΔMTS-TAO enzyme was used to study the activity of new TAO inhibitors based on the 4-hydroxybenzoate and 4-alkoxybenzaldehyde scaffolds (Figure 1). These compounds were designed as analogues of lead compound **1**, a low micromolar TAO inhibitor with potent activity against African trypanosomes [12]. The results of rTAO inhibition analysis, trypanocidal activity against wild type and several multi-drug-resistant strains of trypanosomes, and metabolic stability in mouse serum allowed the production of structure-activity relationships (SAR) with these potent TAO inhibitors and the identification of strong candidates for in vivo studies and preclinical development. This is the first time that not only the problem of local drug concentration is addressed as part of the inhibitor-design for a mitochondrial target in a protozoan parasite, but that it has been demonstrated that inhibitors coupled to such targeting moieties still inhibit the intended target without loss of affinity, and with greatly improved anti-parasite activity and selectivity index.

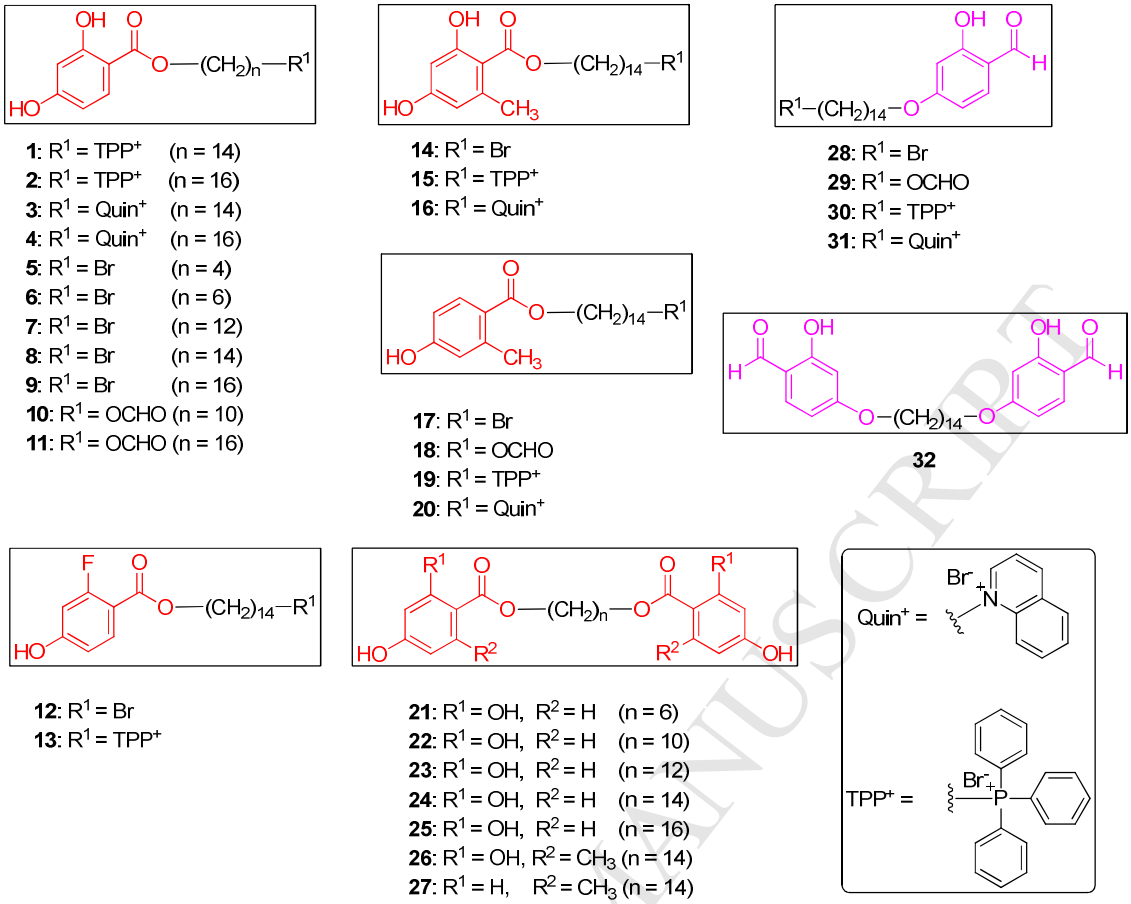

Figure 1. Structure of the TAO inhibitors

2. Results

2.1. Cloning and expression of Trypanosome Alternative Oxidase without mitochondrial targeting sequence (ΔMTS-TAO)

PCR amplification of ΔMTS-TAO and full length (fl) rTAO gave bands on agarose gel corresponding to 915 bp and 990 bp, respectively (Fig. S1A), while the PCR amplification of these TAO genes from the pET101-NHis_6SUMO plasmid, *i.e.* products NHis_6SUMO-ΔMTS-TAO and NHis_6SUMO-fl-TAO gave bands corresponding to 1.26 kb and 1.34 kb, respectively (Fig. S1B). These PCR products were confirmed by sequence analysis to be the correct DNA fragments, and in the correct orientation.

Plasmids with either the full-length or ΔMTS-TAO gene insert were used to transform a heme-deficient strain of *E. coli*, FN102, and the transformants were observed for its viability in the absence of aminolevulinic acid (ALA) in order to verify the ability of the two TAO constructs to complement the absence of terminal oxidase activity in this strain (Fig. 2SA and S2B).

As expected, the result showed that terminal oxidase activity of the heme-deficient *E. coli* FN102 was restored in all native FN102 colonies having the NHis_6SUMO-pET101 plasmid with the TAO insert. There was no visible aerobic growth in the native FN102 in the absence of ALA (Fig. S2A and S2B).

It was also observed that cultures of colonies having the TAO insert plasmid plus 50 µg/mL ALA displayed a better growth pattern than those having the TAO insert plasmid but without ALA and also better than the native FN102 cultures with 50 µg/mL ALA. This observation could be due to TAO restoring the terminal oxidase activities in the native FN102 cells but in addition increasing the total terminal oxidase activities in

native FN102 when the normal heme synthesis pathway was restored in the presence of ALA.

However, there were no significant observable difference in the growth pattern of the FN102 *E. coli* expressing ΔMTS-TAO compared with clones expressing the fl-rTAO gene (Fig. S2A and S2B), showing that both forms are active as a terminal oxidase. This is consistent with our expectation that the MTS is cleaved off upon transportation into the mitochondria in trypanosomes and showed that this recombinant ΔMTS-TAO functioned as a terminal oxidase in the respiratory chain of the heme-deficient FN102 *E. coli* complementing the function of the deleted quinol oxidases.

2.2. Purification of ΔMTS-TAO and *fl*-TAO. rTAO from various stages of purification was subjected to SDS-PAGE analysis. The crude FN102 lysate, a membrane fraction, flow-through, and peak fractions from a TALON column were subjected to discontinuous SDS PAGE (Fig. 2). As expected, a band corresponding to 48 kD, which is the correct size for full length TAO ($NHis_6$SUMO-fl-TAO), was observed in lanes 9 and 10 (duplicate). Removal of $NHis_6$SUMO (11 kD) with the highly efficient SUMO (ULP-1) protease produced the native TAO protein with the expected 37 kD band corresponding to fl-rTAO (Fig. 2). Similarly, the 45 kD band corresponding to $NHis_6$SUMO-ΔMTS-TAO became 34 kD upon cleavage with ULP-1, corresponding to ΔMTS-TAO. Thus, a physiologically active TAO without Mitochondrial Targeting Signal was successfully purified.

The purified ΔMTS-TAO obtained from the column was clear while that of the fl-TAO was slightly turbid; this may be because the MTS is known to be somewhat hydrophobic, reducing solubility. Although the two forms of purified TAO were both very active, the purified ΔMTS-TAO was found to be higher in total and specific

activity than fl-rTAO, and was obtained in higher yield (Table S1). Also, the purified ΔMTS-TAO exhibited a superior purification (10.16-fold) than the fl-TAO (7.91-fold respectively).

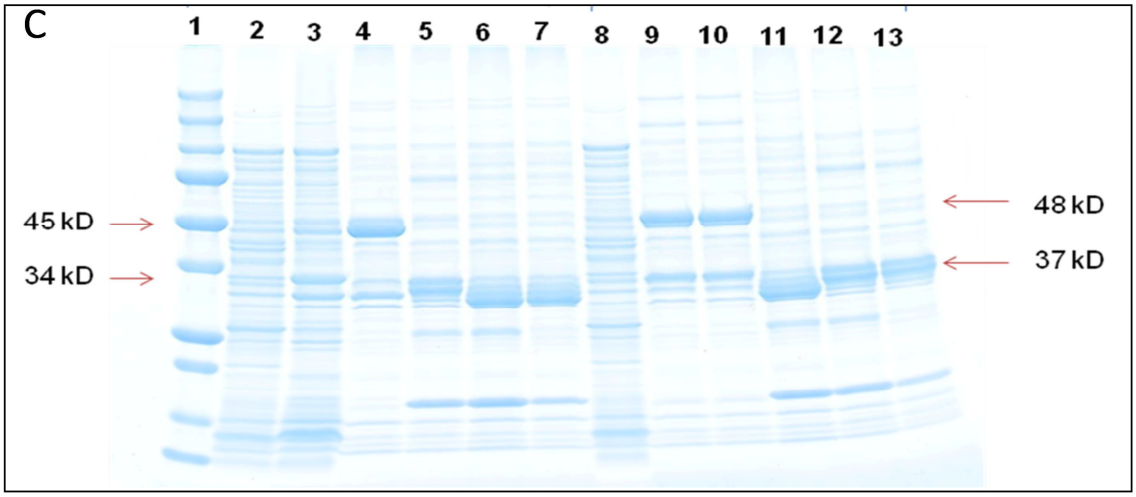

Figure 2. SDS-PAGE for the various purification steps involved in the purification of rTAO from FN102 *E. coli*. Purification process of ΔMTS-TAO and full length (fl) TAO. Lane: 1 = Marker protein (Bio-rad). 2 = Lysed FN102/ $NHis_6$SUMO-ΔMTS-TAO cells. 3 = membrane fraction. 4 = $NHis_6$SUMO-ΔMTS-TAO. 6, 7, and 11 = ΔMTS-TAO ($NHis_6$SUMO is cleaved). 8 = Lysed FN102/$NHis_6$SUMO-fl-TAO cells. 10 = $NHis_6$SUMO-fl-TAO. 5, 12, and 13 = fl-TAO ($NHis_6$SUMO is cleaved). Three µg of protein was loaded onto each lane.

2.3. Synthesis of the inhibitors

The new cationic inhibitors (**13**, **15**, **16**, **19**, and **20**) derived from the 2,4-hydroxybenzoate lead **1** [12] were synthesized in two steps (Scheme 1). The esterification of **33**–**36** with an equimolar amount of a dibromoalkane and sodium bicarbonate in acetonitrile gave a mixture of the bromoalkane intermediate (**5**, **6**, **12**, **14**, **17**) and the dimer product (**21**, **26**, **27**). When dimethylformamide was used as solvent,

the formyl by-product (**18**) was also isolated from the reaction mixture by silica chromatography. The second step consisted in the nucleophilic substitution of the bromoalkane intermediate with either triphenylphosphine or quinoline to give the corresponding triphenylphosphonium (**13**, **15**, **19**) and quinolinium salts (**16**, **20**), respectively. The synthesis of compounds **1**–**4**, **7**–**11**, and **22**–**25** was reported earlier [12].

Scheme 1. Synthesis of 4-Hydroxybenzoate Derivatives[a]

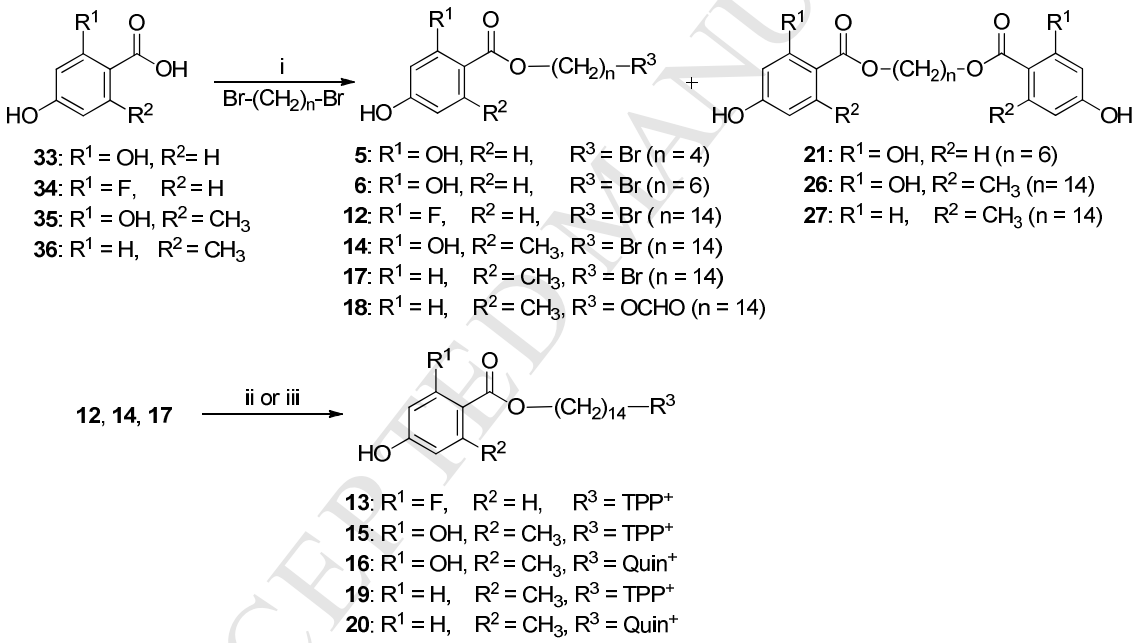

[a]Reagents and conditions: (i) $NaHCO_3$, CH_3CN or DMF, Δ; (ii) Ph_3P, CH_3CN, 80 ºC, 10 days; (iii) quinoline, CH_3CN, 80 ºC, 10 days.

The synthesis of the 2-hydroxybenzaldehyde derivatives **28**–**32** is shown in Scheme 2. Alkylation of 2,4-dihydroxybenzaldehyde with an equimolar amount of 1,14-dibromo tetradecane [16] and $NaHCO_3$ (1 equivalent) in DMF yielded **28**, **29** and **32** that were

isolated by silica chromatography. The cationic derivatives **30** and **31** were obtained by reaction of **28** with Ph_3P and quinoline, respectively (Scheme 2).

Scheme 2. Synthesis of 2-Hydroxybenzaldehyde Derivatives[a]

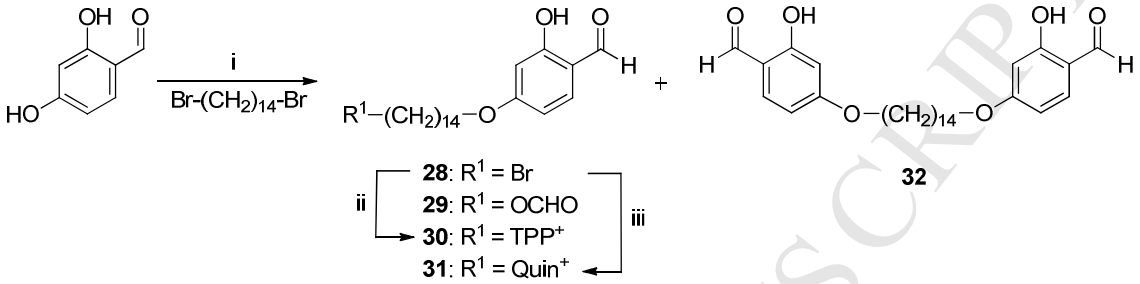

[a]Reagents and conditions: (i) $NaHCO_3$, DMF, 65 ºC, 68 h (ii) Ph_3P, CH_3CN, 80 ºC, 10 days; (iii) quinoline, CH_3CN, 80 ºC, 10 days.

2.4. Inhibition studies with ΔMTS-TAO and SAR of cationic and non-cationic inhibitors

The compounds were tested as inhibitors of the ubiquinol oxidase activity of purified ΔMTS-TAO by recording the absorbance change of ubiquinol-1 at 278 nm. Ascofuranone and SHAM were used as positive controls whereas DMSO was used as negative control. Control experiments were also carried out to check that no auto-oxidation of ubiquinol-1 occurred in the medium. The quality of the purified rTAO was tested in the presence of up to 1 mM ascofuranone, which, at concentrations ≥0.1 µM completely inhibited the conversion of ubiquinol-1 to ubiquinone-1, indicating that no other oxidase was co-purified with TAO. To rule out any possibility that the inhibitors might act non-specifically as iron chelators (i.e. with other heme-containing proteins),

control experiments in the presence and absence of $FeCl_2$ were performed, showing no difference in the extent of TAO inhibition.

Most of the compounds tested against TAO (25 out of 30) displayed submicromolar inhibition. This represents a nearly 1000-fold increase in potency compared with the parent scaffolds **33**–**36** used to design the inhibitors (Table 1). Among these, one compound (**18**) displayed an IC_{50} value of 1.1 ± 0.2 nM, twice as potent as the reference drug ascofuranone, four inhibited TAO with IC_{50} < 10 nM (**14**, **17**, **22**, **23**), and thirteen displayed two-digit nanomolar IC_{50} values. The 2,4-dihydroxybenzoates **1**–**11** inhibited TAO in the low nanomolar (non-cationic derivatives **5**–**11**) to low micromolar range (cationic compounds **1**–**4**). With the non-cationic derivatives, a correlation between inhibitory activity and methylene linker length was observed, the longest linkers giving the best, low nanomolar, inhibitors (C14 > C16 > C12 >> C10 > C6 > C4). For the C16 linker, little difference in activity was observed when changing the R^1 group from a bromine (**9**) to a formiate group (**11**). However, the introduction of a lipocation such as triphenylphosphonium (TPP) (**2**) or quinolinium (**4**) in this position was highly detrimental to TAO inhibition (>500-fold decrease in potency). As regards to cationic inhibitors, a linker with 14 methylene units was preferred (compare **1**/**2** and **3**/**4**). Hence, this linker was chosen to design the rest of the inhibitors for the SAR studies. Importantly, for the 2-fluoro-4-hydroxybenzoate (**13**), 2,4-dihydroxy-6-methylbenzoates (**15, 16**), and 4-hydroxy-2-methylbenzoates (**19**, **20**), the addition of a mitochondrion-targeting lipocation in R^1 barely affected their inhibitory potency against rTAO, showing that the lipocation does not participate in the interaction with the binding pocket (or, at the very least, does not interfere with binding to TAO) when a C14 linker is used.

Concerning the effect of modifications of the phenyl ring substituents R^2 and R^3 on rTAO inhibition, the introduction of a methyl group in R^3 was favorable as shown by the 16- and 13-fold increase in inhibition of **15** and **16** compared to **1** and **3**, respectively. In fact, the presence of a methyl group alone in R^3 (i.e. without OH group in R^2) was sufficient to get nanomolar range inhibitors (**17**–**20**) of similar potencies (compare **14**/**17**, **15**/**19**, **16**/**20**) indicating that the 2-OH group is not essential for binding to TAO within this series. However, the presence of this 2-OH group should not be overlooked for the design of TAO inhibitors as it was essential to get superior metabolic stability in serum when combined with a 6-Me substituent (e.g. compounds **15** and **16**, discussed in section 7). Replacement of the R^3 methyl group by a fluorine atom in the R^2 position was favorable for the cationic TPP derivative (**13** is 2.7-fold more potent than **19**) whereas it was unfavorable for the non-cationic bromo analogue (**12** is 4-fold less potent than **17**).

The 4-formyl-3-hydroxyphenoxy–based inhibitors **28**–**31** were somewhat less potent than the corresponding 4-hydroxybenzoate derivatives (compare **28** with **12**/**14**/**17**, **29** vs **18**, and **30** vs **1**/**13**/**15**/**19**) with the following order of inhibitory potency: R^1 = Br > $^{+}PPh_3$ > OCHO >> quinolinium. Interestingly, the cationic TPP analogue **30** was 5-fold more potent than the quinolinium counterpart **31**.

The 4-hydroxybenzoate dimers (**22**–**27**) inhibited TAO in the low nanomolar range (11–15.7 nM) whereas the 4-formyl-3-hydroxyphenoxy-based dimer **32** was approximately 20-times less potent (IC_{50} = 240 nM) (Table 1). For the dimer series, a linker of 10 to 12 methylene units seemed to be favored (compare **22**/**23** vs **24**/**25**) whereas the nature of R^1 and R^2 was less influential (compare **24** with **26**/**27**).

Table 1. Inhibition of purified rTAO by 4-hydroxy benzoate (**1**–**27**), 4-alkoxy benzaldehyde (**28**–**32**), and 4-hydroxybenzoic acid derivatives (**33**–**36**).

Cmpd	Structure	n	R^1	R^2	R^3	rTAO IC_{50}[a] (µM)
1	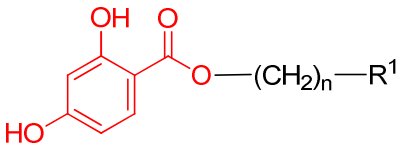	14	$^+PPh_3$	-	-	1.46 ± 0.01
2		16	$^+PPh_3$	-	-	>5
3		14	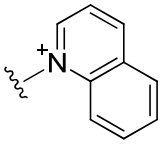	-	-	1.36 ± 0.06
4		16	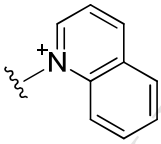	-	-	>5
5		4	Br	-	-	0.45 ± 0.01
6		6	Br	-	-	0.24 ± 0.02
7		12	Br	-	-	0.0174 ± 0.0018
8		14	Br	-	-	0.0108 ± 0.0008
9		16	Br	-	-	0.0124 ± 0.0003
10		10	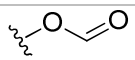	-	-	0.150 ± 0.005
11		16	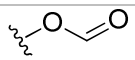	-	-	0.0144 ± 0.0012
12	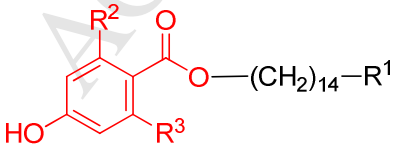		Br	F	H	0.030 ± 0.003
13			$^+PPh_3$	F	H	0.030 ± 0.003
14			Br	OH	CH_3	0.007 ± 0.001
15			$^+PPh_3$	OH	CH_3	0.088 ± 0.013
16			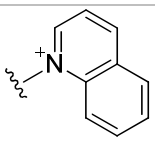	OH	CH_3	0.104 ± 0.011
17			Br	H	CH_3	0.007 ± 0.003
18			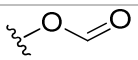	H	CH_3	0.0011 ± 0.0002
19			$^+PPh_3$	H	CH_3	0.081 ± 0.009

20			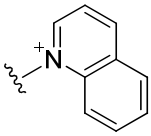	H	CH_3	0.030 ± 0.005
22	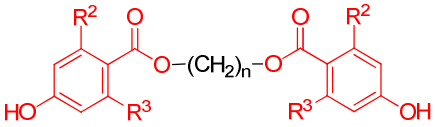	10	-	OH	H	0.0069 ± 0.0001
23		12	-	OH	H	0.0070 ± 0.0001
24		14	-	OH	H	0.0157 ± 0.0013
25		16	-	OH	H	0.0123 ± 0.0041
27		14	-	H	CH_3	0.013 ± 0.003
28	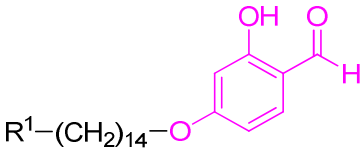		Br	-	-	0.073 ± 0.011
29			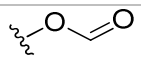	-	-	0.33 ± 0.02
30			$^{+}PPh_3$	-	-	0.22 ± 0.01
31			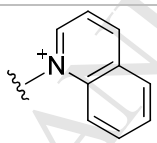	-	-	1.23 ± 0.02
32	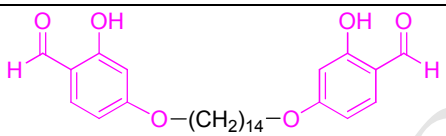		-	-	-	0.24 ± 0.02
33	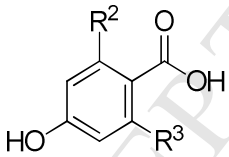		-	OH	H	116 ± 11
34			-	F	H	115 ± 5
35			-	CH_3	OH	143 ± 6
36			-	CH_3	H	112 ± 4
AF[b]						0.0020 ± 0.0004
SHAM[c]						5.93 ± 0.13

[a] Purified recombinant trypanosome alternative oxidase from *T. b. brucei* (n = 3). [b]Ascofuranone. [c] Salicylhydroxamic acid.

2.5. Kinetics and inhibitory mechanism of compounds on ΔMTS-TAO

A set of 5 representative TAO inhibitors were selected for kinetic assays and to determine the type of inhibition with purified ΔMTS-TAO. The results were used to construct the Michaelis-Menten plots (Supplementary Fig. S3) which were transformed to Lineweaver–Burk plots. The K_m and V_{max} value for the uninhibited reaction was obtained as 384.3 ± 11.7 µM and 53.2 ± 6.6 µmol/min/mg, respectively, while the apparent K_m (K_m^{App}) values for the inhibited reactions ranged from 464 to 1644 µM. The K_i values were obtained from secondary plots (slopes of reciprocal plots *vs* inhibitor concentrations) of the Lineweaver–Burk plots, the values were 71.4, 870, 4.1, 52.9, and 34.1 nM for **11**, **15**, **18**, **20**, and **22**, respectively. The Lineweaver–Burk analysis indicated that, similar to SHAM [17], compounds **11** and **22** inhibit TAO non-competitively whereas compounds **15**, **18**, and **20** were competitive inhibitors (Figure 3). It is notable that all the inhibitors that bound competitively were 2-methyl-4-hydroxylbenzoates, whereas both compounds that produced a non-competitive plot lacked the 2-methyl group; this seems to indicate a somewhat different binding mode for the 2-methylbenzoates; the tail group, in contrast, does not seem to determine whether the binding mode is competitive or not.

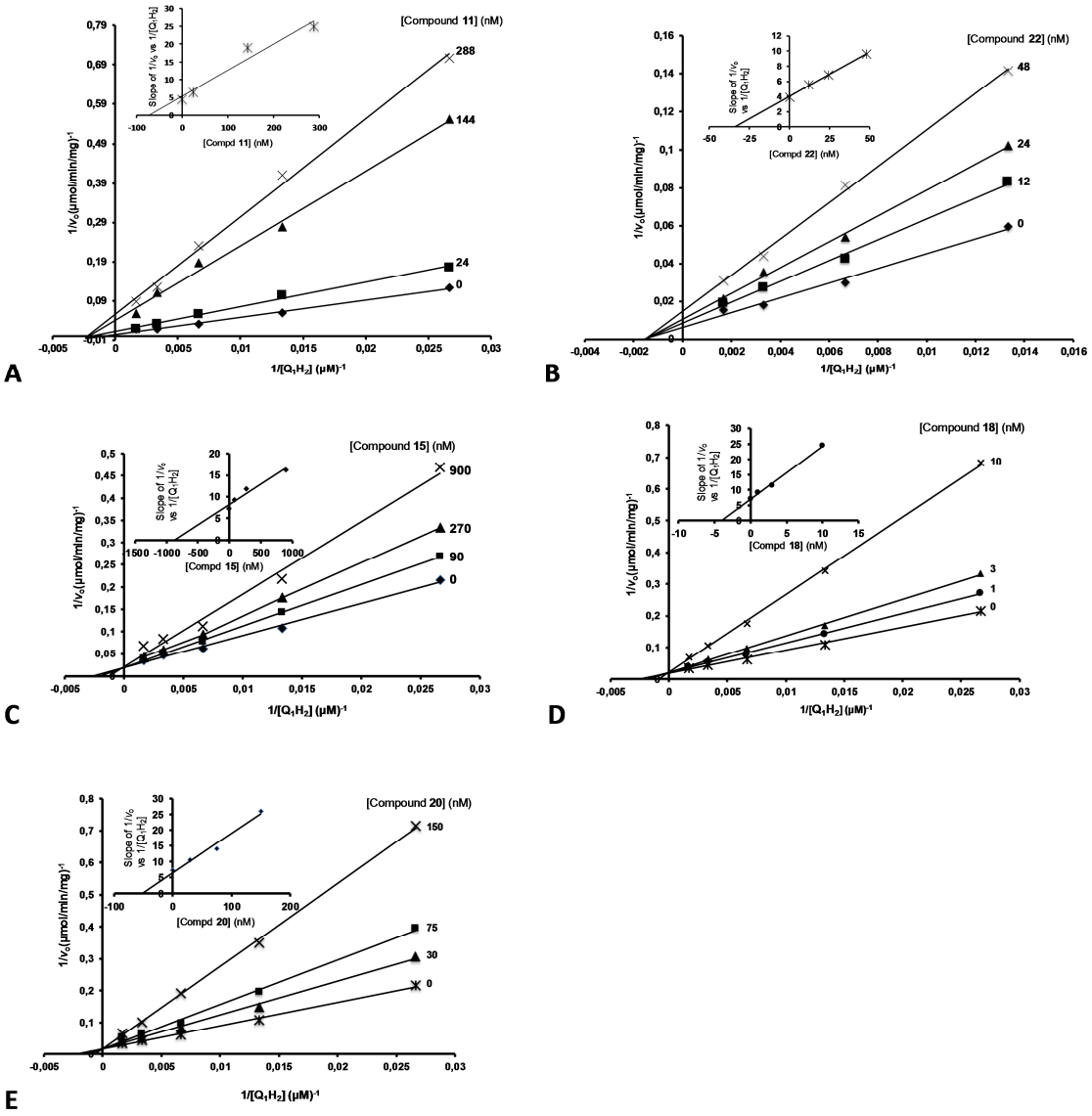

Figure 3. Inhibitory mechanism of compounds on ΔMTS-TAO and determination of inhibitory constants K_i. Kinetic assays of TAO were carried out in the presence of varying amounts of compounds **11**, **15**, **18**, **20**, and **22**. Lineweaver–Burk plots, $1/v_o$ (μmol/min/mg protein)$^{-1}$ vs 1/[ubiquinol] (μM)$^{-1}$ revealed the inhibition mechanisms, and the secondary plots (insets), slopes of Lineweaver–Burk plots *vs* [inhibitor concentration] (μM) were used to estimate the of K_i for the inhibitors **11** (panel A), **22** (B), **15** (C), **18** (D), and **20** (E).

2.6. In vitro activity against *T. b. brucei* and *T. congolense* wild type strains

As TAO is essential for parasite viability, inhibition of TAO should inhibit parasite respiration and growth. Hence, the in vitro activities of the inhibitors were determined against wild type (WT) *T. brucei* and *T. congolense*, and against various drug-resistant *T. brucei* strains, using a resazurin-based assay (Tables 2–3). The cationic inhibitors were the most effective against *T. brucei* WT, with EC_{50} values ranging from 0.00058 µM (**13**) to 1.75 µM (**31**). The TPP derivatives **15**, **19**, and **30**, displaying single-digit nanomolar EC_{50} values, were between 13 and 87-fold more potent than their quinolinium counterparts **16**, **20**, and **31** in these whole-cell assays; similar ratios were seen against *T. congolense*. The 4-formyl-3-hydroxyphenoxy-based inhibitors (**30**, **31**) were the least active of these series with EC_{50} of 0.13 and 1.75 µM, respectively, a result that correlated with a lower inhibitory action on ΔMTS-TAO (0.22 and 1.23 µM, respectively).

The non-cationic TAO inhibitors displayed much lower activity against *T. brucei*, with EC_{50} values in the micromolar range. The formiate derivatives (**11**, **18**, and **29**) were approximately 3-times more potent than the bromo analogues (**9**, **17**, and **28**) whereas the dimer compounds (**21**–**27**, **32**) were only weakly effective against *T. brucei* (IC_{50} > 25 µM). These results were not unexpected as the compounds lack the mitochondrion-targeting lipocation group, and the reduced activity probably results from poor accumulation in the mitochondrion of the parasite and possibly poor cellular penetration as well. The relatively low solubility of the dimeric compounds may also help explain the lack of in vitro activity against the parasite.

Co-incubation with glycerol, which inhibits the *T. brucei* anaerobic ATP production pathway [18], significantly ($P<0.05$) potentiated the trypanocidal activities of most of

the compounds including SHAM, whereas it had no apparent effect on the efficacy of **16**, **18**, **19**, or on the effects of control drugs pentamidine and diminazene (Table 2). These results are consistent with the aerobic glycolytic pathway being affected by these compounds, which is expected for compounds inhibiting TAO. The anomalous results of compounds **16**, **18** and **19**, all 2-methyl-4-hydroxybenzoates, that were not enhanced in the presence of extracellular glycerol, may be due to a multi-target activity against *T. brucei*, making them less dependent than the other compounds on inhibition of TAO alone (see discussion).

Cytotoxicity against human cells was low (CC_{50} > 200 µM) resulting in selectivity indices from > 8 (for non-cationic compounds) to between 110 and 344,000 for the cationic derivatives (**15**, **16**, **19**, **20**, **30**, and **31**).

The TAO inhibitors were consistently approximately 3-times less active against the *T. congolense* IL3000 strain than against *T. brucei* WT, but followed the same overall trends of inhibitor potency, and there was excellent correlation between the two sets of EC_{50} values (r^2 = 0.95; Figure S4), showing that the compounds act on both species through a similar process. The systematic difference may be explained by a lesser degree of reliance on TAO by *T. congolense*, which is believed to have a slightly more complex mitochondrion than *T. brucei*. Nevertheless, three cationic TPP compounds (**13**, **15** and **19**) were 5- to 40-fold more potent than the reference drug diminazene against this parasite species.

Table 2. EC_{50} values (μM) against Wild Type Strains of *T. b. brucei*, *T. congolense*, and Cytotoxicity against Human Cells ($CC_{50,}$ μM).

Cmpd	***T. b. brucei* WT**[a]	SI[b]	***T. b. brucei* WT** (+ 5 mM glycerol)	RF[c]	t-test[d]	***T. congolense* WT**[e]	SI[f]	**Human cells**[g]
5	NE, 400		NE, 400			nd[h]		>200
6	17.7 ± 0.5	>11	12.1 ± 0.5	0.68	1.5E-3	72.9 ± 22.5	>2.7	>200
7	14.5 ± 1.0	>27	6.2 ± 0.3	0.42	8.6E-4	52.1 ± 3.7	>7.7	>400[i]
9	45.7 ± 1.5	>8	11.1 ± 0.7	0.24	8.6E-6	>100		>400[i]
10	31.8 ± 0.9	>12	17.5 ± 0.9	0.55	1.2E-4	>100		>400[i]
11	11.9 ± 1.6	>34	5.1 ± 0.5	0.43	2.5E-2	>100		>400[i]
12	14.7 ± 0.1	>13	7.19 ± 0.07	0.49	1E-6	>50		>200
13	0.00058 ± 0.00001	>344,000	0.00039 ± 0.00003	0.66	5.5E-3	0.018 ± 0.005	>11,000	>200
14	14.6 ± 0.2	>13	7.71 ± 0.03	0.53	6E-6	>100		>200
15	0.0016 ± 0.0005	>125,000	0.0014 ± 0.0001	0.92	8.1E-1	0.005 ± 0.001	>40,000	>200
16	0.032 ± 0.0006	>6250	0.071 ± 0.002	2.22	2.1E-5	nd		>200
17	14.4 ± 0.1	>13	7.5 ± 0.1	0.52	1E-6	nd		>200
18	4.1 ± 0.1	>48	7.8 ± 0.4	1.92	7.5E-4	nd		>200
19	0.0024 ± 0.0008	>83,000	0.0032 ± 0.0005	1.32	4.4E-1	0.039 ± 0.015	>5128	>200
20	0.21 ± 0.02	>952	0.145 ± 0.007	0.69	5.6E-2	1.82 ± 0.45	>110	>200
22	49.0 ± 7.8	>8	12.2 ± 0.6	0.25	1.5E-2	>100		>400[i]
23	32.9 ± 0.9	>12	13.6 ± 1.2	0.41	4.0E-5	>100		>400[i]
24	42.1 ± 2.9	>9	15.9 ± 1.5	0.38	7.5E-4	>100		>400[i]
25	26.7 ± 5.5	>15	12.4 ± 0.3	0.46	8.0E-2	>100		>400[i]
27	NE, 400		NE, 400			NE, 400		>200
28	17.6 ± 0.5	>11	10.7 ± 0.5	0.61	8.8E-4	42.6 ± 6.3	>4.6	>200
29	3.8 ± 0.1	>52	1.80 ± 0.01	0.48	7.2E-5	nd		>200
30	0.133 ± 0.003	>1503	0.067 ± 0.005	0.51	4.8E-4	0.27 ± 0.12	>740	>200
31	1.75 ± 0.01	>114	1.23 ± 0.08	0.70	2.6E-3	2.1 ± 0.7	>95	>200
32	NE, 400		NE, 400			NE, 400		>200
33[j]	17.1 ± 1.0		nd			nd		nd

SHAM[k]	38.7 ± 4.8	7.0 ± 0.3	0.18	1.36E-11		
Pentamidine	0.0033 ± 0.0004	0.004 ± 0.0008	1.14	6.3E-1		
Diminazene	0.065 ± 0.007	0.063 ± 0.002	0.97	8.4E-1	0.20 ± 0.08	
PAO[l]	0.0011 ± 0.00003					0.29 ± 0.02

[a]Trypomastigotes of *T. b. brucei* s427 ($n \geq 4$). [b]Selectivity index (SI) = CC_{50}/EC_{50} (*T. brucei* WT). [c]Resistance factor relative to WT without glycerol: RF = EC_{50} (in the presence of glycerol)/EC_{50} (without glycerol). [d]Unpaired Student's t-test comparing EC_{50} values against the WT strain in the presence and absence of 5 mM glycerol. [e]Trypomastigotes of *T. congolense* IL3000 ($n \geq 2$). [f]Selectivity index (SI) = CC_{50}/EC_{50} (*T. congolense* WT). [g]Cytotoxicity on Human Foreskin Fibroblast (HFF) cells (n = 2). [h]Not determined. [i]Human embryonic kidney cells (n = 3). [j]2,4-Dihydroxybenzoic acid. [k]Salicylhydroxamic acid. [l]Phenylarsine oxide. Note: the MIC value for ascofuranone has been reported as 30 nM in the presence of glycerol and 250 µM under standard growth conditions [8].

Table 3. EC_{50} values (μM) against resistant strains of *T. b. brucei.*

Cmpd	***T. b. brucei* AQP2/3-ddKO**[a]	RF[b]	t-test[c]	***T. b. brucei* AQP triple KO**[d]	RF	t-test	***T. brucei* B48**[e]	RF
5	NE, 400			NE, 400			NE, 400	
6	11.6 ± 0.6	0.65	9.2E-4	12.1 ± 0.14	0.68	3.7E-4	20.5 ± 1.8	1.2
7	10.0 ± 0.1	0.69	1.2E-2	4.7 ± 0.3	0.32	4.1E-4	14.9 ± 1.0	1.03
9	14.5 ± 0.7	0.32	1.5E-5	5.1 ± 0.2	0.11	3.2E-6	49.0 ± 0.6	1.07
10	27.4 ± 0.7	0.86	1.7E-2	15.6 ± 0.4	0.49	3.3E-5	22.1 ± 4.1	0.69
11	5.0 ± 0.1	0.42	2E-2	1.27 ± 0.07	0.11	3E-3	13.0 ± 3.7	1.1
12	6.8 ± 0.1	0.46	1E-6	7.0 ± 0.2	0.48	5E-6	17.3 ± 0.2	1.2
13	0.00025 ± 0.00013	0.43	1.2E-2	0.00037 ± 0.00005	0.64	1.7E-2	0.00075 ± 0.00005	1.3
14	7.30 ± 0.01	0.50	5E-6	6.8 ± 0.3	0.47	2.3E-5	15.6 ± 0.2	1.1
15	0.0008 ± 0.0002	0.51	2.6E-1	0.0014 ± 0.0001	0.89	7.4E-1	0.0019 ± 0.0003	1.2
16	0.035 ± 0.003	1.11	1.2E-1	0.03 ± 0.01	0.87	6.9E-1	0.089 ± 0.001	2.8
17	7.1 ± 0.2	0.49	1E-6	7.2 ± 0.6	0.50	2E-4	14.4 ± 0.2	1.0
18	1.40 ± 0.04	0.34	1.4E-5	1.8 ± 0.2	0.45	2.8E-4	4.44 ± 0.02	1.1
19	0.0022 ± 0.0001	0.92	8.4E-1	0.005 ± 0.003	2.0	4.8E-1	0.0022 ± 0.0001	0.9
20	0.10 ± 0.01	0.47	1.7E-2	0.086 ± 0.005	0.41	6.2E-3	0.30 ± 0.03	1.4
22	24.6 ± 0.6	0.50	7E-2	7.1 ± 0.8	0.14	8E-3	41.6 ± 5.5	0.85
23	26.7 ± 1.8	0.81	1.9E-2	8.9 ± 0.6	0.27	4.7E-6	33.6 ± 1.0	1.0
24	28.2 ± 1.2	0.67	1.1E-2	14.8 ± 0.2	0.35	4.6E-4	36.6 ± 0.9	0.87
25	14.3 ± 0.8	0.54	1.2E-1	9.3 ± 0.3	0.35	4.4E-2	31.9 ± 8.0	1.2
27	NE, 400			NE, 400			NE, 400	
28	8.4 ± 0.2	0.48	8.5E-5	7.9 ± 0.4	0.45	1.4E-4	15.5 ± 0.8	0.9
29	1.4 ± 0.1	0.38	5.6E-5	1.82 ± 0.02	0.48	8E-5	3.6 ± 0.2	1.0
30	0.042 ± 0.005	0.32	6.1E-4	0.053 ± 0.006	0.40	3.6E-4	0.11 ± 0.02	0.8
31	0.95 ± 0.03	0.54	4.7E-4	1.08 ± 0.03	0.62	2.4E-5	2.35 ± 0.15	1.3
32	NE, 400			NE, 400			NE, 400	
33[f]	nd			16.6 ± 0.9	0.96	4.4E-1	nd	
SHAM[g]	31.9 ± 0.9	0.82	3.6E-1	8.9 ± 0.4	0.23	4.3E-3	nd	
Pentamidine	0.047 ± 0.003	14.1	1E-4	0.064 ± 0.006	19.2	6E-4	0.94 ± 0.03	285

Diminazene						0.78 ± 0.04	12
PAO[h]	0.0013 ± 0.00004	1.17	2E-2	0.0013 ± 0.00003	1.11	4.4E-2	

[a]*T. brucei* cell lines from which both aquaporins AQP2 and AQP3 have been knocked out. [b]Resistance factor relative to WT. [c]Unpaired Student's t-test comparing EC_{50} values against the WT strain. [d]*T. brucei* cell line from which *all* aquaporins were knocked out. [e]*T. b. brucei* strain resistant to pentamidine, diminazene, and melaminophenyl arsenicals. [f]2,4-Dihydroxybenzoic acid. [g]Salicylhydroxamic acid. [h]Phenylarsine oxide.

2.7. In vitro activity against *T. brucei* aquaglyceroporin-deficient strains

Very little difference in activity was observed between WT and the multidrug resistant cell line B48 (resistant to diamidines including diminazene and pentamidine, some nucleoside analogues and to melaminophenyl arsenicals) [19, 20], with resistance factors (RF) consistently close to 1, whereas resistance to the control drugs diminazene and pentamidine was 12- and 285-fold respectively (Table 3). In contrast, most of the inhibitors were significantly more effective against the *T. brucei* cell lines from which both aquaporins AQP2 and AQP3 (AQP2/3-ddKO) [21] or all three *T. brucei* aquaporins were deleted (AQP1-3 triple KO) [22]. The effect of the compounds on the AQP knockout lines may be explained by a shift in metabolism of trypanosomes in the presence of the TAO inhibitors. Inhibition of TAO forces the parasite to produce large quantities of glycerol to survive anaerobically, producing ATP via glycerol kinase by substrate phosphorylation [23, 24]. In the absence of aquaglyceroporins, trypanosomes are not able to efficiently dispose of that glycerol resulting in the inhibition of the glycerol kinase and higher susceptibility to the TAO inhibitors. Indeed, the RF factors of EC_{50}s in the presence of glycerol or in the absence of aquaporins were in close agreement (r^2= 0.89 with two outliers of $RF_{(glycerol)}$ ~2).

2.8. Metabolic stability of the inhibitors in mouse and horse sera

The metabolic stability of five cationic benzoate derivatives (**3**, **13**, **15**, **16**, **19**, and **20**) to esterases was assessed in mouse serum to assess the degree of in vivo hydrolysis of the ester bond over time. The stability of the 4-hydroxybenzaldehyde analogue (**30**), which cannot be metabolized by esterases, was also measured for comparison. The test compounds and the control drug were incubated at 37 ºC in mouse serum over a 24 h period and the quantity of compound recovered intact at different times (0.25, 0.5, 1, 2,

and 24 h) was quantified by HPLC–MS (Figure S5) [25]. The compounds resulting from the hydrolysis of the ester bond [i.e. benzoic acids **33**–**36**, (14-hydroxytetradecyl)triphenylphosphonium, and 1-(14-hydroxytetradecyl)quinolin-1-ium] were the only metabolites detected by HPLC–MS.

The 2,4-dihydroxy-6-methyl benzoate derivatives (**15**, **16**) were very stable in mouse serum with <20% hydrolysis after 24 h of incubation at 37 ºC (ditialzem: half-life ≈ 24 h). In contrast, the 2-methyl-4-hydroxy derivatives (**19**, **20**) were >99% hydrolyzed after 24 h with an approximate half-life of 60 min and 30 min, respectively. This result was similar to the 2-hydroxy analogue **3**, 50% of which was hydrolyzed after 1 h of incubation. The 2-fluoro analogue **13** was the most sensitive to esterases with a half-life <15 min. As expected, the 4-hydroxybenzaldehyde analogue (**30**), which has no ester bond, was not hydrolyzed in mouse serum (i.e. same amount recovered intact at t = 15 min and t = 24 h). However, a large proportion of **30** was bound to serum proteins (≈ 90%) as shown by the percentage of compound recovered intact after 15 min (12%) which was maintained steady over 24 h (Figure S5). This result may be related to Schiff base formation between the aldehyde group and the amino groups of the serum proteins.

Some differences in the rate of metabolism were observed between mouse and horse sera. In an experiment with 2 time points (2 h, 24 h) performed with horse serum (data not shown), <30% of **15** and <40% of **16** were hydrolyzed after 24h of incubation whereas <20% of **19** was hydrolyzed after 2 h of incubation (compared with approximately 70% in mouse serum). Ditialzem was completely hydrolyzed after 24 h in this medium (1% recovered).

2.9. Microsomal stability

Compounds **15** and **16** (5 µM) were exposed to human liver fractions, S9 fraction and human liver microsomes, to investigate in vitro microsomal stability. Both compounds were stable and did not suffer phase 1 metabolism with P450 enzymes/NADPH when compared with standard diclofenac (Table S2). Contrarily to **16**, compound **15** did suffer phase 2 metabolism in presence of the S9 fraction and cofactor UDPGA with half-live of approximately 2 h. Altogether, these results suggest metabolic stability for these benzoate derivatives, confirming the observed in vivo stability in serum.

2.10. Molecular Docking Studies. Predicted TAO binding modes

Three bromo compounds, which only differ in the nature of the aromatic head (**14**, **17**, **28**) were chosen to obtain information on the binding mode of the aromatic head without the interference of the tail substituent. Likewise, in order to study the influence of the tail on the TAO binding mode, three compounds with the same aromatic head (i.e. 2-methyl-4-hydroxybenzoate: **17**, **19**, **20**) but different tails (i.e. bromine, TPP or quinolinium lipocations) were studied. Compound **5**, with a short C4 linker was also studied for comparison.

Compounds **5**, **14**, **17**, **19**, **20**, and **28** were docked into the ubiquinol binding cavity of TAO using the coordinates of the TAO–AF2779OH complex [PDB ID code: 3VVA] [26]. AF2779OH (5-chloro-3-[(2E,6E)-8-hydroxy-3,7-dimethylnona-2,6-dienyl]-2,4-dihydroxy-6-methylbenzaldehyde) is an ascofuranone (AF) derivative comprised of a substituted aromatic head and an isoprenoid tail but lacking the furanone ring. Similar to the structures of AF and its derivatives, the scaffold of the TAO inhibitors reported here consists of an aromatic head and a C14 methylene tail.

The modelled structures revealed that analogs **14**, **17**, **19**, **20**, and **28** aligned perfectly at the head portion of AF2779-OH and, to a large extent, along their linkers. We observed

that the linker length was important for effective binding of the inhibitor into the enzyme cavity. The 14-methylene linker of all the inhibitors proved optimal for allowing the head portion access to the catalytic center (distance <5 Å). In contrast, the 4-methylene linker of compound **5** was too short and resulted in reduced interactions with the hydrophobic region of the enzyme cavity, which may explain its lower inhibitory potency. In this predicted binding pattern, the inhibitors occupy the hydrophobic pocket of TAO close to the catalytic center via its head portion, while the tail extends outward into the solvent (Figure 4A,B). In addition to the hydrogen bond (HB) interactions of the carbonyl oxygen atom with the amino acids that form the active site (Arg96, Arg118 and Thr219), the 4-OH of the aromatic head of inhibitors **14**, **17**, **19**, and **20**, and the aldehyde oxygen of **28** are in close proximity to the diiron center (Figure 4A,C-E); for compounds **17**, **19**, and **20** the methyl at position R^3 is favored as it engages in hydrophobic interactions with a number of residues including Leu122, Ala216, and Thr219 (Figure 4C). For compound **14**, the 2-OH group at position R3 interacts via hydrogen bonding (HB) with Arg118 and Thr219 (Figure 4D). In contrast, no direct contact was revealed at the R^2 position, where there seems to be opportunity for further derivatization (Figure 4C,D).

As regards to the 2-hydroxybenzaldehyde derivative **28**, its aromatic head binds TAO in a slightly different way: the aldehyde group engages in two HBs with Glu122 and Tyr220 whereas the 2-OH substituent forms one HB with Tyr220. In addition, it is noteworthy that the ether O atom of the molecule interacts with only one residue of the active site (HB with Arg118) in contrast to the benzoate derivatives, which carbonyl O atom engage in HBs with 3 residues of the active site (Figure 4E-F). These differences could possibly explain the 10-fold lower inhibition potency of the benzaldehyde derivatives compared with the 4-hydroxybenzoate inhibitors.

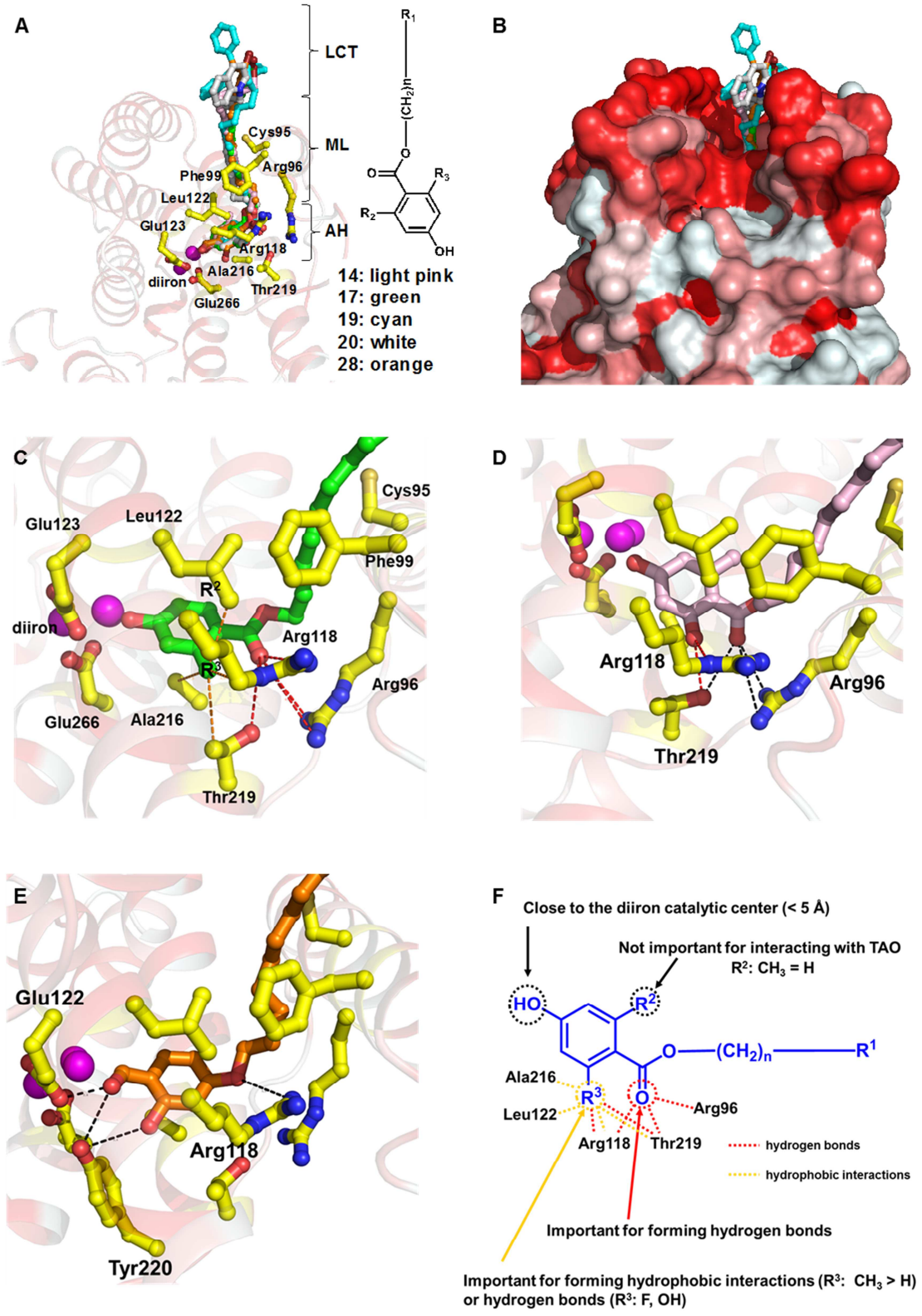

Figure 4. Modeled structure of derivatives **14** (R^2 = CH_3, R^3 = OH), **17**, **19**, **20** (R^2 = H, R^3 = CH_3), and **28** in the TAO active site. (A) Structural model of the TAO-inhibitors

complex. AH, ML, and LCT mean aromatic head, methylene linker (spacer), and lipocation tail, respectively. Compounds **14**, **17**, **19, 20** and **28** are shown in light pink, green, cyan, white, and orange stick models, respectively. The residues within 4 Å distance of the compounds are shown in ball-and-stick models. (B) Surface model of the TAO-inhibitors complex. Compounds **17**, **19**, and **20** are shown in green, cyan and white stick models, respectively. In the surface model, red and white show hydrophobic and hydrophilic regions, respectively. The tail region of the compounds is exposed to the solvent. (C) Close-up view of the active site for compound **17**. The red and orange dashed lines are hydrogen bonds and hydrophobic interactions, respectively. (D) Close-up view of the active site for compound **14** showing the hydrogen bonds (dashed lines) of the 2-OH (R^3) and the carbonyl group with Arg96, Arg118, and Thr219. (E) Close-up view of the active site for compound **28**. Hydrogen bonds appear as dashed lines. (F) Schematic drawing for the predicted interactions between the 4-hydroxybenzoate inhibitors (**13**, **14**, **17**, **19**, **20**) and TAO.

3. Discussion

The TAO gene contains 990 nucleotides, encoding a protein of 330 amino acids including the N-terminal 25 amino acid residue Mitochondrial Targeting Signal (MTS). For the majority of mitochondrial proteins, their transport into the mitochondria relies on two key fundamentals: (i) the presence of an MTS in the protein sequence and (ii) the presence of specific translocators in the mitochondrial membrane domain that recognize the specific signals [27]. Three main types of MTS have been found in proteins that are intended for delivery into the mitochondria: a stop-transfer or sorting signal, an internal signal, and N-terminal targeting sequence [28], which is an amphipathic helix of hydrophobic and basic amino acid residues that is usually cleaved after transportation of the protein to the mitochondria [15]. Consequently, the physiological and functional TAO is without MTS [27] but to date only the full length protein has been studied, despite problems of low stability, poor solubility and yield, and poor X-ray diffraction resolution of TAO crystals attributed to the MTS [26].

Because the full length TAO is not the physiologically active form in BSF *T. brucei*, it is important to study ΔMTS-TAO instead, especially when designing inhibitors for potential therapeutic intervention.

Here we report the first expression and purification of ΔMTS-TAO, and show that it was substantially more soluble, stable and active than fl-TAO, and could be purified at a higher yield. This ΔMTS-TAO enzyme was then used to characterize the inhibitory efficacy of 32 cationic and non-cationic compounds and develop structure-activity relationships with these series of 4-hydroxybenzoate and 4-alkoxybenzaldehyde derivatives.

We have previously reported the synthesis and characterization of 3 series of lipophilic cation (LC) conjugates based on SHAM and 2,4-DHBA scaffolds. These compounds were designed so as to efficiently target the mitochondrion of *T. brucei*, using either the flat heterocyclic 1-quinolinium cation or the bulky TPP cation as mitochondrion targeting moieties [12]. The findings from our previous report, providing a preliminary analysis of their structure-activity relationships (SAR), allowed the design and synthesis of the potent 4-hydroxybenzoate and 4-alkoxybenzaldehyde TAO inhibitors reported in the current paper. Similarly to the previously reported series [12], the presence of a mitochondrion-targeting lipophilic cation was essential to obtain nanomolar activity against trypanosomes. However, when this was included, the trypanocidal activity was very impressive, with several compounds displaying EC_{50} values below that of the benchmark drug pentamidine, and 13 showing sub-nanomolar activity, while displaying no cross-resistance with the critical diamidine and melaminophenyl arsenical classes of trypanocides. Moreover, the compounds were similarly active, and displayed the same SAR, against *T. brucei*, whose subspecies *T. b. gambiense* and *T. b. rhodesiense* cause the human form of African sleeping sickness,

and *T. congolense*, the main pathogen of livestock in sub-Saharan Africa. For *T. congolense*, several compounds displayed activities much superior to the most-widely used drug, diminazene aceturate, with EC_{50} values up to 40-fold lower for **15**, at 5 nM, and no observed toxicity on the control human cell line at concentrations up to 200 μM, as well as metabolic stability in serum. It is clear that the compounds here reported hold extraordinary promise for both human and animal trypanosomiasis.

The presence of the lipocation hardly affected the inhibitory potency against TAO (4- to 10-fold), showing that the lipocation barely interferes with binding to TAO when a C14 linker is used. Although a strict correlation between EC_{50} against trypanosomes and inhibition of TAO was not observed, the measured IC_{50} values against ΔMTS-TAO are compatible with a mode of action via TAO inhibition.

The higher susceptibility of the aquaporin-deficient *T. brucei* cell lines towards the test compounds (and SHAM) supports the hypothesis that these TAO inhibitors act on *T. brucei* through inhibition of TAO as designed, as the anaerobic pathway that is the cell's only option for ATP-production when TAO is inhibited, produces intracellular glycerol in large quantities. In aquaporin-deficient trypanosomes, glycerol builds up in the cells, leading to the inhibition of glycerol kinase and the final route of ATP production [22]. The reason that the cells have to resort to the anaerobic production of glycerol upon inactivation of TAO is that the typical electron transport chain and oxidative phosphorylation present in mammalian cells are not operational in bloodstream form trypanosomes (BSFs). Consequently, the BSFs depend largely on glycolysis for its ATP generation. During aerobic respiration, BSFs produce a net of two molecules of ATP per glucose via glycolysis, which is dependent on the unique activity of TAO to regenerate NAD^+. But when TAO is inhibited or during anaerobiosis, there is a metabolic shift in favor of glycerol production, aided by glycerol

kinase (GK) activity, producing a net of only one ATP from each glucose molecule consumed by the BSFs. Under these conditions, GK becomes critical for the survival of BSFs. The production of ATP by the trypanosome's GK is via transphosphorylation of ADP with glycerol 3-phosphate (G3P) [24, 29, 30]. Therefore, co-administration of the TAO inhibitors and glycerol, or accumulation of glycerol in aquaporin-deficient *T. brucei* cell-lines, kills the parasites more effectively [31], as the glycerol competes with G3P, inhibiting the production of ATP by mass action [24].

However, as noted in sections 5 and 6, the trypanocidal activities of compounds **16** (i.e. 2,4-dihydroxy-6-methyl benzoate derivative), **18** and **19** (i.e. 2-methyl-4-hydroxybenzoates), were not enhanced in the presence of extracellular glycerol, and likewise the activities of **16** and **19** were not enhanced in the AQP knockout lines, although the activity of **18** was highly significantly enhanced against the AQP knockout lines. Of these, **18**, in particular, is an excellent inhibitor of rTAO, although **16** and **19** also display submicromolar IC_{50} values (Table 1). We conclude that some of the most potent 2(6)-methyl derivatives, particularly **16** and **19**, display a multi-target activity against *T. brucei*, making them less dependent than the other compounds on inhibition of TAO alone; both compounds contain the cationic tail group that will make them accumulate strongly in the mitochondrion. In the case of compound **19**, which shows a lower metabolic stability in serum ($t_{1/2} \approx 60$ min), hydrolysis by cytosolic esterases to generate the much less active derivative 2-methyl-4-hydroxybenzoic acid (**36**: IC_{50} = 111.6 µM) in addition to (14-hydroxytetradecyl)triphenylphosphonium metabolites, both poor inhibitors of TAO, could also explain the lower dependence of this compound on inhibition of TAO alone. Of interest, the glycerol sensitization was largest in the TAO inhibitor SHAM (5.5-fold; Table 2), similar to the EC_{50} shift in the AQP triple knockout (4.4-fold; Table 3). The less exclusive reliance on TAO inhibition by some of

the lipocation-coupled 2-methyl-4-hydroxybenzoates seems not to have increased toxicity to human cells, and would help prevent the development of drug resistance.

The kinetics of our test compounds binding to TAO as determined by Lineweaver-Burk plot analysis indicated a non-competitive inhibition for the 2,4-dihydroxybenzoate derivatives (**11**, **22**), and a competitive inhibition for the 2-methyl-4-hydroxy benzoates (**15**, **18**, and **20**). Interestingly, compounds **15**, **18**, and **20** with a C14 linker were all competitive inhibitors, independently of the terminal tail group (i.e. TPP, formiate and quinolinium group, respectively), indicating that they interact with the TAO enzyme in a similar way. These data were supported by the docking experiments which showed that the 14-methylene linker was optimal for allowing the head portion access to the catalytic center. In contrast, the 2,4-dihydroxybenzoate derivatives with a C16 (formiate **11)** and C10 linker (dimer **22**) were noncompetitive inhibitors as shown by Lineweaver-Burk plot analysis. Crystallographic analysis is being attempted with representative compounds in order to resolve the exact binding modes of the two classes of inhibitors. Some of the inhibitors showed nanomolar IC_{50} values against ΔMTS-TAO in the same range as ascofuranone (IC_{50} = 2 nM; Table 1), which has also been reported to noncompetitively inhibit the ubiquinol-dependent O_2 consumption of *T. b. brucei* (K_i = 2.38 nM) [32]. Similarly, SHAM was reported to inhibit TAO with a non-competitive (mixed type) mode of inhibition similar to the one reported here for compounds **11** and **22** [23]. Such uncompetitive patterns were also observed by Clarkson and co-workers with different series of *p*-alkoxybenzhydroxamic acids, 3,4-dihydroxybenzoates, and *N*-n-alkyl-3,4-dihydroxybenzamides having alkyl chains of 10 to 12 carbons [33].

The TAO inhibitors reported here are benzoate derivatives that are potentially prone to hydrolysis by esterases *in vivo*. However, the metabolism experiments showed that subtle changes in the structure allow control over the *in vivo* stability of the

inhibitors in serum. From our results, it is clear that the substituents in the *ortho* position relative to the ester bond are crucial to modulate the sensitivity of the compounds to serum hydrolases. Increased stability was obtained for (2-OH, 6-Me) > 2-Me ≈ 2-OH >> 2-F. These modifications to the scaffold also improved the inhibitory potency against TAO by one order of magnitude [e.g. (2-OH,6-Me) ≈ 2-Me > 2-F >> 2-OH] and positively (**13**, **15**, **16**) or negatively (**19**, **20**) affected the trypanocidal activity by 1- to 3-fold with respect to the parent compounds **1** and **3**. Hence, the 2,4-dihydroxy-6-methyl TAO inhibitors **15** and **16**, which are metabolically stable in serum and in microsomal fractions, and display single digit nanomolar trypanocidal activity and selectivity over human cells (SI > 6000), represent good candidates for *in vivo* studies in mouse models of trypanosomiasis.

The activity of **15** and **16** against the human parasite *T. b. rhodesiense* STIB900 (IC_{50} = 5 and 72 nM, respectively) was confirmed in vitro. Hence, a preliminary in vivo experiment in mice infected with *T. b. rhodesiense* STIB900/luc expressing the red-shifted luciferase gene [34] showed that compounds **15** and **16** reduced the parasitemia by 95% 24 h after the last treatment (Table S3). Even though no cures were obtained at the modest dose tested (4×10 mg/kg ip), these promising results warrant further investigations with this class of compounds.

4. Conclusion

The reported procedure for the high yield expression of ΔMTS-TAO that is substantially more soluble, stable, and active, than fl-TAO is a helpful tool for the development of new TAO inhibitor drug candidates. We have successfully developed a class of potent and selective new hits active against human (*T. brucei* spp.) and

veterinary (*T. congolense*) African trypanosomes, and confirmed their designed mode of action as inhibition of TAO. This was accomplished by efficiently targeting the compounds to the trypanosome's mitochondrion, thereby increasing the potency of the original small molecule inhibitors against *T. brucei* by up to 3 orders of magnitude. Importantly, the inhibitors with the 2,4-dihydroxy-6-methyl scaffold (e.g. **15**, **16**), which are metabolically stable in serum and in liver fractions, were active in the STIB900 mouse model of acute infection and are promising candidates for further in vivo studies.

5. Experimental section

5.1. Chemistry. Anhydrous solvents were purchased to Aldrich/Fluka in SureSeal™ bottles and used as received. Thin Layer chromatography (TLC) was performed on silica gel 60 F254 aluminum TLC plates (MERCK). Medium pressure silica chromatography was performed on a FlashMaster Personal system using FlashPack SI prepacked columns (2, 5, 10, 20, and 50 g). Melting points were measured with a Reichert-Jung Thermovar apparatus and are uncorrected. LC-MS spectra were recorded on a WATERS apparatus integrated with a HPLC separation module (2695), PDA detector (2996) and Micromass ZQ spectrometer. Three different cone voltages were used (20, 40 and 60 ēV) and detection was in positive or negative mode (ES^+ or ES^-). Analytical HPLC was performed with a SunFire C18-3.5 μm column (4.6 mm × 50 mm). Mobile phase A: CH_3CN + 0.08% formic acid and B: H_2O + 0.05% formic acid. UV detection was carried over 190 to 440 nm. ^1H NMR and ^{13}C NMR spectra were registered on a Bruker Avance-300, Varian Inova-400, Varian-Mercury-400, and Varian-system-500 spectrometers. Chemical shifts of the ^1H NMR spectra were referenced to tetramethylsilane (δ 0) for $CDCl_3$ or the residual proton resonance of the

deuterated solvents: DMSO-d_6 (δ 2.50), CD_3CN (δ 1.94), and CD_3OD (δ 3.31). Chemical shifts of the ^{13}C NMR spectra were referenced to $CDCl_3$ (δ 77.16), DMSO-d_6 (δ 39.52), CD_3CN (δ 1.32), and CD_3OD (δ 49.0). Coupling constants *J* are expressed in hertz (Hz). Accurate mass was measured with an Agilent Technologies Q-TOF 6520 spectrometer using electrospray ionization. All of the biologically tested compounds were ≥ 95% pure by HPLC.

5.1.1. General procedure for the synthesis of the bromoalkane intermediates (5, 6, 12, 14, 17, 28) and dimers (21, 26, 27, 32). A Kimax tube was charged with an equimolar quantity of benzoic acid **33**–**37** (1.3 mmol, 1 equiv.), sodium bicarbonate (1.3 mmol, 1 equiv), and the dibromoalkane (1.3 mmol, 1 equiv.) in anhydrous acetonitrile or DMF (10 mL). The tube was flushed with argon, stopped, and the reaction mixture was stirred at 65 ºC or 90 ºC for the time indicated in each case. The solvent was evaporated under vacuum to give a crude solid residue. The different products were isolated by silica chromatography (5g SI prepacked column) using hexane/EtOAc (100/0 → 50/50) as eluent. The structure of the obtained isomer (i.e. the benzoate product and not the 4-alkyloxy-substituted benzoic acid isomer) was checked by ^{1}H–^{13}C HMBC and NOESY experiments.

4-Bromobutyl 2,4-dihydroxybenzoate (5). Following the general procedure 5.1.1. starting from 1,4-dibromobutane (0.305 g, 1.95 mmol) and using CH_3CN as solvent (20 mL). The reaction mixture was heated at 65 ºC for 66 h. Compound **5** was isolated by silica chromatography using hexane/EtOAc (98/2) as eluent. White solid (202 mg, 36%). HPLC (UV): 100%. ^{1}H NMR (300 MHz, $CDCl_3$) δ 10.94 (s, 1H), 7.66 (d, *J* = 8.4 Hz, 1H), 6.38 – 6.24 (m, 2H), 5.63 (br s, 1H), 4.28 (t, *J* = 6.0 Hz, 2H), 3.41 (t, *J* = 6.2 Hz, 2H), 2.04 – 1.80 (m, 4H). ^{13}C NMR (75 MHz, $CDCl_3$) δ 170.0, 163.8, 162.1, 132.0,

108.0, 106.0, 103.3, 64.2, 33.2, 29.4, 27.4. LRMS (ES^+) *m/z* 289 $(M+H)^+$. HRMS (ESI^+) *m/z* 287.9988 ($C_{11}H_{13}BrO_4$ requires 287.9997).

6-Bromohexyl 2,4-dihydroxybenzoate (6). Following the general procedure 5.1.1. starting from 1,6-dibromohexane (300 mg, 1.95 mmol) and using CH_3CN as solvent (20 mL). The reaction mixture was heated at 65 ºC for 4 days. Compounds **6** and **21** were isolated by silica chromatography using hexane/EtOAc as eluent. Compound **6** eluted with hexane/EtOAc:90/10 and **21** with hexane/EtOAc:75/25. Compound **6**: yellowish oil (203 mg, 25%); HPLC (UV) > 95 %. ^{1}H NMR (300 MHz, $CDCl_3$) δ 11.06 (s, 1H), 7.73 (dd, *J* = 8.6 Hz, 1H), 6.39 (dd, *J* = 2.5, 8.6 Hz, 1H), 6.36 (d, *J* = 2.5 Hz, 1H), 5.40 (s, 1H), 4.32 (t, *J* = 6.5 Hz, 2H), 3.42 (t, *J* = 6.7 Hz, 2H), 2.00 – 1.65 (m, 4H), 1.61 – 1.37 (m, 4H). ^{13}C NMR (75 MHz, $CDCl_3$) δ 170.2, 163.7, 161.9, 132.0, 108.0, 106.1, 103.3, 65.1, 33.9, 32.7, 28.6, 27.9, 25.4. LRMS (ESI^+) *m/z* 317, 319 $(M+H)^+$. HRMS (ESI^+) *m/z* 316.0315 ($C_{13}H_{17}BrO_4$ requires 316.0310).

14-Bromotetradecyl 2-fluoro-4-hydroxybenzoate (12). Following the general procedure 5.1.1. starting from 1,14-dibrotetradecane (67 mg, 0.19 mmol) and using CH_3CN as solvent (20 mL). The reaction mixture was heated at 90 ºC for 22 days. Compound **12** was isolated by preparative plate chromatography on silica using hexane/EtOAc (8/2) as eluent. Beige solid (16 mg, 20%); mp 42 – 48 ºC. HPLC (UV) > 95 %. ^{1}H NMR (300 MHz, $CDCl_3$) δ 10.95 (s, 1H), 7.66 (d, *J* = 9.5 Hz, 1H), 6.46 – 6.19 (m, 2H), 4.24 (t, *J* = 6.5 Hz, 1H), 3.91 (t, *J* = 6.4 Hz, 1H), 3.35 (t, *J* = 6.6 Hz, 2H), 1.97 – 0.57 (m, 24H). ^{13}C NMR (75 MHz, $CDCl_3$) δ 170.2, 165.2, 164.0, 131.3, 108.0, 105.6, 101.3, 68.1, 33.9, 33.8, 32.8, 32.7, 29.0, 28.01, 27.96, 25.4. LRMS (ESI^+) *m/z* 431, 433 $(M+H)^+$. HRMS (ESI^+) *m/z* 430.1516 ($C_{21}H_{32}BrFO_3$ requires 430.1519).

14-Bromotetradecyl 2,4-dihydroxy-6-methylbenzoate (14). Following the general procedure 5.1.1. starting from 1,14-dibrotetradecane (530 mg, 1.49 mmol) and using CH_3CN as solvent (15 mL). The reaction mixture was heated at 90 ºC for 48 h. The products were isolated by silica chromatography. Compound **14** eluted with hexane/EtOAc:95/5 and **26** with hexane/EtOAc:85/15. Compound **14**: colorless solid (155 mg, 26%); mp 62.5 – 64.7 ºC. HPLC (UV) > 95 %. ^{1}H NMR (300 MHz, $CDCl_3$) δ 11.84 (s, 1H), 6.21 (d, *J* = 2.8 Hz, 1H), 6.16 (d, *J* = 2.8 Hz, 1H), 5.53 (brs, 1H), 4.26 (t, *J* = 6.5 Hz, 2H), 3.34 (t, *J* = 6.8 Hz, 2H), 2.43 (s, 3H), 1.93 – 1.67 (m, 4H), 1.52 – 1.14 (m, 20H). ^{13}C NMR (75 MHz, $CDCl_3$) δ 172.0, 165.5, 160.3, 144.1, 111.4, 106.0, 101.4, 65.7, 34.2, 33.0, 29.72, 29.66, 29.61, 29.57, 29.3, 28.9, 28.7, 28.3, 26.3, 24.6. LRMS (ESI^+) *m/z* 443, 445 $(M+H)^+$. HRMS (ESI^+) *m/z* 442.1709 ($C_{22}H_{35}BrO_4$ requires 442.1719).

14-Bromotetradecyl 4-hydroxy-2-methylbenzoate (17). Following the general procedure 5.1.1. starting from 1,14-dibrotetradecane (470 mg, 1.32 mmol) and using DMF as solvent (10 mL). The reaction mixture was heated at 65 ºC for 68 h. The products were isolated by silica chromatography. Compounds **17** and **27** eluted with hexane/EtOAc:90/10, and **18** with hexane/EtOAc:80/20. Compound **17**: colorless solid (41 mg, 7%); mp 54.4 – 57.3 ºC. HPLC (UV) > 95 %. ^{1}H NMR (400 MHz, $CDCl_3$) δ 7.82 (d, *J* = 9.3 Hz, 1H), 6.66 – 6.60 (m, 2H), 5.55 (br, 1H), 4.19 (t, *J* = 6.7 Hz, 2H), 3.33 (t, *J* = 6.9 Hz, 2H), 2.50 (s, 3H), 1.78 (p, *J* = 7.0 Hz, 2H), 1.66 (h, *J* = 7.1 Hz, 2H), 1.4 – 1.1 (m, 20H). ^{13}C NMR (100 MHz, $CDCl_3$) δ 167.6, 158.8, 143.5, 133.4, 122.3, 118.5, 112.8, 64.9, 34.2, 33.0, 29.9, 29.74, 29.70, 29.67, 29.66, 29.58, 29.4, 28.9, 28.3, 26.3, 22.4. LRMS (ESI^+) *m/z* 427, 429 $(M+H)^+$. HRMS (ESI^+) *m/z* 426.1790 ($C_{22}H_{35}BrO_3$ requires 426.1770).

14-(Formyloxy)tetradecyl 4-hydroxy-2-methylbenzoate (18). Yellowish solid (31 mg, 6%); mp 59.0 – 60.5 ºC. HPLC (UV) > 95 %. ^{1}H NMR (300 MHz, $CDCl_3$) δ 8.00 (s, 1H), 7.86 – 7.75 (m, 1H), 6.66 – 6.60 (m, 2H), 6.36 (br s, 1H), 4.18 (t, *J* = 6.5 Hz, 2H), 4.10 (t, *J* = 6.6 Hz, 2H), 2.49 (s, 3H), 1.70 – 1.53 (m, 4H), 1.34 – 1.15 (m, 20H). ^{13}C NMR (75 MHz, $CDCl_3$) δ 167.8, 161.7, 159.2, 143.4, 133.4, 122.0, 118.5, 112.8, 65.0, 64.5, 29.8, 29.7, 29.64, 29.61, 29.5, 29.37, 29.28, 28.9, 28.6, 26.4, 26.3, 25.9, 22.4. LRMS (ESI^+) *m/z* 393 $(M+H)^+$. HRMS (ESI^+) *m/z* 392.2548 ($C_{23}H_{36}O_5$ requires 392.2563).

Hexane-1,6-diyl bis(2,4-dihydroxybenzoate) (21). Colorless solid (5.8 mg, 0.7%); mp 68 – 80 ºC. HPLC (UV) > 91 %. ^{1}H NMR (300 MHz, $CDCl_3$+CD_3OD) δ 7.61 (d, *J* = 9.4 Hz, 2H), 6.46 – 6.00 (m, 4H), 4.83 (br s, 2H), 4.24 (t, *J* = 6.5 Hz, 4H), 1.73 (t, *J* = 6.6 Hz, 4H), 1.58 – 1.31 (m, 4H). ^{13}C NMR (75 MHz, $CDCl_3$+CD_3OD) δ 170.2, 163.8, 163.4, 131.7, 108.3, 104.9, 102.7, 64.8, 28.6, 25.8. LRMS (ESI^+) *m/z* 391 $(M+H)^+$. HRMS (ESI^+) *m/z* 390.1296 ($C_{20}H_{22}O_8$ requires 390.1315).

Tetradecane-1,14-diyl bis(2,4-dihydroxy-6-methylbenzoate) (26). Colorless solid (29.6 mg, 5%); HPLC (UV) = 87%. ^{1}H NMR (300 MHz, DMSO-d_6) δ 10.90 (br s, 2H), 10.02 (br s, 2H), 6.25 – 6.06 (m, 4H), 4.22 (t, *J* = 6.5 Hz, 4H), 2.30 (s, 6H), 1.73 – 1.58 (m, 4H), 1.46 – 1.16 (m, 20H). ^{13}C NMR (75 MHz, $CDCl_3$+ CD_3OD) δ 170.2, 161.8, 161.3, 141.1, 110.5, 107.0, 100.5, 64.8, 29.05, 28.97, 28.6, 28.1, 25.6, 22.5, 21.3. LRMS (ESI^+) *m/z* 531 $(M+H)^+$. HRMS (ESI^+) *m/z* 530.2874 ($C_{30}H_{42}O_8$ requires 530.2880).

Tetradecane-1,14-diyl bis(4-hydroxy-2-methylbenzoate) (27). Colorless solid (15 mg, 6.6%); mp 42 – 46 ºC. HPLC (UV) > 95 %. ^{1}H NMR (300 MHz, CD_3OD) δ 7.82 (d, *J* = 9.3 Hz, 2H), 6.74 (m, 2H), 6.64 (d, *J* = 6.6 Hz, 2H), 4.21 (t, *J* = 6.5 Hz, 4H), 2.51

(s, 6H), 1.73 (t, *J* = 7.1 Hz, 4H), 1.49 – 1.03 (m, 20H). ^{13}C NMR (75 MHz, CD_3OD) δ 168.8, 161.5, 143.8, 133.9, 121.3, 118.9, 113.3, 65.3, 30.3, 30.22, 30.20, 29.9, 29.4, 26.8, 22.6. LRMS (ESI^+) *m/z* 499 $(M+H)^+$. HRMS (ESI^+) *m/z* 498.2995 ($C_{30}H_{42}O_6$ requires 498.2981).

4-((14-Bromotetradecyl)oxy)-2-hydroxybenzaldehyde (28). Following the general procedure 5.1.1. starting from 1,14-dibrotetradecane (385 mg, 1.1 mmol) and using DMF as solvent (10 mL). The reaction mixture was stirred at 65 ºC for 24 h, and 68 h at room temperature. The products **28**, **29** and **32** were isolated by silica chromatography using hexane/EtOAc:97/3. Compound **28**: colorless solid (17 mg, 4%); mp 55.5 – 58.6 ºC. HPLC (UV) > 95 %. ^{1}H NMR (300 MHz, $CDCl_3$) δ 11.41 (s, 1H), 9.64 (s, 1H), 7.35 (d, *J* = 8.6 Hz, 1H), 6.46 (dd, *J* = 2.4, 8.6 Hz, 1H), 6.34 (d, *J* = 2.4 Hz, 1H), 3.93 (t, *J* = 6.6 Hz, 2H), 3.34 (t, *J* = 6.9 Hz, 2H), 1.82 – 1.69 (m, 4H), 1.23 (m, 20H). ^{13}C NMR (75 MHz, $CDCl_3$) δ 194.4, 166.6, 164.7, 135.3, 115.2, 108.9, 101.2, 68.8, 34.2, 33.0, 29.9, 29.74, 29.68, 29.6, 29.5, 29.1, 28.9, 28.3, 26.1. LRMS (ESI^+) *m/z* 413, 415 $(M+H)^+$. HRMS (ESI^+) *m/z* 412.1621 ($C_{21}H_{33}BrO_3$ requires 412.1613).

14-(4-Formyl-3-hydroxyphenoxy)tetradecyl formate (29). Yellowish solid (40 mg, 9%); mp 63.5 – 68.8 ºC. HPLC (UV) > 95 %. ^{1}H NMR (300 MHz, $CDCl_3$) δ 11.41 (s, 1H), 9.63 (s, 1H), 7.99 (s, 1H), 7.34 (d, *J* = 8.7 Hz, 1H), 6.45 (dd, *J* = 2.4, 8.7 Hz, 1H), 6.34 (d, *J* = 2.4 Hz, 1H), 4.09 (t, *J* = 7.1 Hz, 2H), 3.93 (t, *J* = 6.5 Hz, 2H), 1.82 – 1.04 (m, 24H). ^{13}C NMR (75 MHz, $CDCl_3$) δ 194.4, 166.6, 164.7, 161.4, 135.3, 115.1, 108.9, 101.2, 68.7, 64.3, 29.84, 29.69, 29.68, 29.63, 29.4, 29.3, 29.1, 28.64, 28.57, 26.1, 26.0. LRMS (ESI^+) *m/z* 379 $(M+H)^+$. HRMS (ESI^+) *m/z* 378.2417 ($C_{22}H_{34}O_5$ requires 378.2406).

4,4'-(Tetradecane-1,14-diylbis(oxy))bis(2-hydroxybenzaldehyde) (32). Colorless solid (12 mg, 3%); mp 111 – 112.8 ºC. HPLC (UV) > 95 %. ^{1}H NMR (300 MHz, $CDCl_3$) δ 11.46 (s, 2H), 9.69 (s, 2H), 7.40 (d, *J* = 8.7 Hz, 2H), 6.51 (dd, *J* = 2.4, 8.7 Hz, 2H), 6.39 (d, *J* = 2.4 Hz, 2H), 3.98 (t, *J* = 6.6 Hz, 4H), 1.83 – 1.20 (m, 24H). ^{13}C NMR (75 MHz, $CDCl_3$) δ 194.4, 166.6, 164.7, 135.3, 115.2, 108.9, 101.2, 68.8, 29.8, 29.77, 29.71, 29.5, 29.1, 26.1. LRMS (ESI^+) *m/z* 471 $(M+H)^+$. HRMS (ESI^+) *m/z* 470.2667 ($C_{28}H_{38}O_6$ requires 470.2668).

5.1.2. General procedure for the synthesis of the triphenylphosphonium (13, 15, 19, 30) and quinolinium salts (16, 20, 31). A Kimax tube was charged with an equimolar amount of the bromoalkane derivative (**5**, **6**, **12**, **14**, **17**, **28**; ≈30 mg, 1 equiv.) and triphenylphosphine (procedure 5.1.2.1) or quinoline (procedure 5.1.2.2) in anhydrous acetonitrile (0.5 mL). The tube was flushed with argon, stopped and the reaction mixture was stirred at 80 ºC for several days. The products were purified by recrystallization as described below.

(14-((2-Fluoro-4-hydroxybenzoyl)oxy)tetradecyl)triphenylphosphonium bromide (13). Following the general procedure 5.1.2.1 the reaction mixture was heated at 80 ºC for 7 days. The solvent was removed under vacuum and **13** was obtained as brown solid (18 mg, 86%) by recrystallization from CH_2Cl_2/hexane. HPLC (UV) > 95 %. ^{1}H NMR (400 MHz, CD_3OD) δ 7.85 – 7.72 (m, 16H), 6.64 (dd, *J* = 2.4, 8.7 Hz, 1H), 6.54 (dd, *J* = 2.4, 12.9 Hz, 1H), 4.26 (t, *J* = 6.5 Hz, 2H), 3.44 – 3.33 (m, 2H), 1.80 – 1.60 (m, 4H), 1.54 (p, *J* = 7.0 Hz, 2H), 1.49 – 1.21 (m, 18H). ^{13}C NMR (101 MHz, CD_3OD) δ 166.0 (d, *J* = 3.8 Hz), 165.1 (d, *J* = 12.2 Hz), 165.0 (d, *J* = 258 Hz), 136.3 (d, *J* = 3.1 Hz), 134.8 (d, *J* = 10.0 Hz), 134.5 (d, *J* = 2.7 Hz), 131.5 (d, *J* = 12.7 Hz), 120.0 (d, *J* = 86.3 Hz), 112.6 (d, *J* = 2.7 Hz), 110.7, 104.5 (d, *J* = 24.7 Hz), 65.9, 31.6 (d, *J* = 16.1 Hz), 30.6, 30.58, 30.52, 30.47, 30.3 (d, *J* = 12.5 Hz), 29.8, 29.7, 27.0, 23.5 (d, *J* = 4.5 Hz),

22.7 (d, *J* = 50.8 Hz). LRMS (ESI^+) *m/z* 613 $(M)^+$. HRMS (ESI^+) *m/z* 613.3243 ($C_{39}H_{47}FO_3P$ requires 613.3247).

(14-((2,4-Dihydroxy-6-methylbenzoyl)oxy)tetradecyl)triphenylphosphonium bromide (15). Following the general procedure 5.1.2.1 the reaction mixture was heated at 80 ºC for 12 days. The solvent was removed under vacuum and **15** was obtained as colorless solid (42.6 mg, 97%) by recrystallization from CH_2Cl_2/hexane; mp 128 – 129 ºC. HPLC (UV) > 95 %. ^1H NMR (500 MHz, CD_3OD) δ 7.89 (td, *J* = 1.8, 7.2 Hz, 3H), 7.83 – 7.72 (m, 12H), 6.19 (d, *J* = 2.4 Hz, 1H), 6.14 (d, *J* = 2.4 Hz, 1H), 4.33 (t, *J* = 6.5 Hz, 2H), 3.42 – 3.34 (m, 2H), 2.46 (s, 3H), 1.82 – 1.73 (m, 2H), 1.66 (h, *J* = 8.0 Hz, 2H), 1.54 (p, *J* = 7.3 Hz, 2H), 1.50 – 1.42 (m, 2H), 1.42 – 1.22 (m, 16H). ^{13}C NMR (75 MHz, CD_3OD) δ 173.1, 166.3, 163.7, 144.4, 136.3 (d, *J* = 3.6 Hz), 134.8 (d, *J* = 10.1 Hz), 131.5 (d, *J* = 12.7 Hz), 120.0 (d, *J* = 86.2 Hz), 112.5, 105.8, 101.8, 66.3, 31.6 (d, *J* = 15.7 Hz), 30.62, 30.57, 30.5, 30.4, 30.3, 30.2, 29.9, 29.7, 27.2, 24.5, 23.5 (d, *J* = 4.4 Hz), 22.7 (d, *J* = 51.0 Hz). LRMS (ESI^+) *m/z* 625 $(M)^+$. HRMS (ESI^+) *m/z* 625.3465 ($C_{40}H_{50}O_4P$ requires 625.3447).

1-(14-((2,4-Dihydroxy-6-methylbenzoyl)oxy)tetradecyl)quinolin-1-ium bromide (16). Following the general procedure 5.1.2.2 the reaction mixture was heated at 80 ºC for 12 days. The precipitate was collected by filtration and rinsed with cold CH_3CN to give **16** as brown solid (19.5 mg, 57%); mp 167 – 168 ºC. HPLC (UV) > 95 %. ^1H NMR (300 MHz, CD_3OD) δ 9.40 (d, *J* = 6.0 Hz, 1H), 9.19 (d, *J* = 8.4 Hz, 1H), 8.52 (d, *J* = 9.0 Hz, 1H), 8.42 (dd, *J* = 1.5, 8.6 Hz, 1H), 8.35 – 8.23 (m, 1H), 8.07 (td, *J* = 6.5, 9.4, 10.1 Hz, 2H), 6.22 – 6.08 (m, 2H), 5.07 (t, *J* = 7.7 Hz, 2H), 4.31 (t, *J* = 6.5 Hz, 2H), 2.46 (s, 3H), 1.75 (q, *J* = 6.9 Hz, 2H), 1.52 – 1.13 (m, 22H). ^{13}C NMR (75 MHz, CD_3OD) δ 172.9, 166.1, 163.4, 150.0, 148.9, 144.3, 137.3, 132.1, 131.6, 131.3, 122.9, 119.4, 112.4, 101.6, 66.1, 59.3, 31.0, 30.8, 30.41, 30.37, 30.34, 30.3 (m), 30.0, 29.5,

27.3, 27.0, 24.6, 24.2. LRMS (ESI^+) *m/z* 492 $(M)^+$. HRMS (ESI^+) *m/z* 492.3128 ($C_{31}H_{42}NO_4$ requires 492.3114).

(14-((4-Hydroxy-2-methylbenzoyl)oxy)tetradecyl)triphenylphosphonium bromide (19). Following the general procedure 5.1.2.1 the reaction mixture was heated at 80 ºC for 10 days. The solvent was removed under vacuum and **19** was obtained as beige hygroscopic solid (35 mg, 82%) by recrystallization from CH_2Cl_2/hexane. HPLC (UV) > 95 %. ^{1}H NMR (500 MHz, CD_3OD) δ 7.89 (td, *J* = 1.8, 7.1 Hz, 3H), 7.78 (m, 16H), 6.65 (d, *J* = 2.5 Hz, 1H), 6.64 – 6.61 (m, 1H), 4.23 (t, *J* = 6.5 Hz, 2H), 3.44 – 3.34 (m, 2H), 2.51 (s, 3H), 1.74 (p, *J* = 6.7 Hz, 2H), 1.66 (h, *J* = 8.1 Hz, 2H), 1.54 (p, *J* = 7.2 Hz, 2H), 1.48 – 1.40 (m, 2H), 1.40 – 1.22 (m, 16H). ^{13}C NMR (75 MHz, CD_3OD) δ 168.9, 162.3, 144.1, 136.2 (d, *J* = 3.4 Hz), 134.8 (d, *J* = 9.9 Hz), 134.1, 131.5 (d, *J* = 12.7 Hz), 121.6, 120.0 (d, *J* = 86.2 Hz), 119.2, 113.7, 65.5, 31.6 (d, *J* = 16 Hz), 30.71, 30.61, 30.55, 30.50, 30.4, 30.3, 29.9, 29.8, 27.2, 24.2, 23.5 (d, *J* = 4.5 Hz), 22.7 (d, *J* = 51 Hz), 22.5. LRMS (ESI^+) *m/z* 609 $(M)^+$. HRMS (ESI^+) *m/z* 609.3499 ($C_{40}H_{50}O_3P$ requires 609.3498).

1-(14-((4-Hydroxy-2-methylbenzoyl)oxy)tetradecyl)quinolin-1-ium bromide (20). Following the general procedure 5.1.2.2 the reaction mixture was heated at 80 ºC for 10 days. The precipitate was collected by filtration and rinsed with cold CH_3CN to give **20** as brown solid (21 mg, 63%); mp 145 – 146 ºC. HPLC (UV) > 95 %. ^{1}H NMR (300 MHz, CD_3OD) δ 9.43 (d, *J* = 5.8 Hz, 1H), 9.21 (d, *J* = 8.4 Hz, 1H), 8.55 (d, *J* = 9.0 Hz, 1H), 8.44 (dd, *J* = 1.5, 8.1 Hz, 1H), 8.30 (ddd, *J* = 1.6, 6.9, 8.8 Hz, 1H), 8.19 – 7.98 (m, 2H), 7.80 (d, *J* = 8.5 Hz, 1H), 6.68 – 6.56 (m, 2H), 5.09 (t, *J* = 7.7 Hz, 2H), 4.22 (t, *J* = 6.5 Hz, 2H), 2.50 (s, 3H), 2.15 – 2.02 (m, 2H), 1.73 (p, *J* = 6.9 Hz, 2H), 1.42 – 1.25 (m, 20H). ^{13}C NMR (75 MHz, CD_3OD) δ 169.0, 162.2, 150.2, 149.0, 144.1, 139.4, 137.3, 134.1, 132.1, 131.7, 131.4, 123.0, 121.6, 119.6, 119.2, 113.6, 65.5, 59.4, 31.1, 30.6,

30.54, 30.47, 30.4, 30.2, 30.1, 29.8, 27.4, 27.1, 22.5. LRMS (ESI^+) *m/z* 476 $(M)^+$. HRMS (ESI^+) *m/z* 476.3165 ($C_{31}H_{42}NO_3$ requires 476.3165).

(14-(4-Formyl-3-hydroxyphenoxy)tetradecyl)triphenylphosphonium bromide (30). Following the general procedure 5.1.2.1 the reaction mixture was heated at 80 ºC for 10 days. The solvent was removed under vacuum and **30** was obtained as colorless solid (25.5 mg, 71%) by recrystallization from CH_2Cl_2/EtOAc; mp 82 – 94 ºC. HPLC (UV) > 95 %. ^1H NMR (500 MHz, CD_3OD) δ 9.77 (s, 1H), 7.92 – 7.86 (m, 3H), 7.83 – 7.73 (m, 12H), 7.57 (d, *J* = 8.7 Hz, 1H), 6.57 (dd, *J* = 2.4, 8.7 Hz, 1H), 6.42 (d, *J* = 2.4 Hz, 1H), 4.04 (t, *J* = 6.4 Hz, 2H), 3.42 – 3.35 (m, 2H), 1.82 – 1.74 (m, 2H), 1.71 – 1.61 (m, 2H), 1.54 (p, *J* = 7.3 Hz, 2H), 1.50 – 1.43 (m, 2H), 1.41 – 1.21 (m, 16H). ^{13}C NMR (75 MHz, CD_3OD) δ 195.6, 167.9, 165.4, 136.3 (d, *J*= 3.2 Hz), 136.2, 134.8 (d, *J*= 10.0 Hz), 131.5 (d, *J*= 12.7 Hz), 120.0 (d, *J*= 86.6 Hz), 116.8, 109.3, 102.0, 69.6, 31.6 (d, *J*= 16.2 Hz), 30.7, 30.6, 30.5, 30.4, 30.35, 30.1, 29.9, 27.0, 23.5 (d, *J*= 4.3 Hz), 22.7 (d, *J*= 50.8 Hz). LRMS (ESI^+) *m/z* 595 $(M)^+$. HRMS (ESI^+) *m/z* 595.3346 ($C_{39}H_{48}O_3P$ requires 595.3341).

1-(14-(4-Formyl-3-hydroxyphenoxy)tetradecyl)quinolin-1-ium bromide (31). Following the general procedure 5.1.2.2 the reaction mixture was heated at 80 ºC for 10 days. The solvent was removed under vacuum and **31** was obtained as beige solid (10 mg, 36%) by recrystallization from CH_2Cl_2/EtOAc; mp 118 – 122 ºC. HPLC (UV) > 95 %. ^1H NMR (300 MHz, CD_3OD) δ 9.77 (s, 1H), 9.46 – 9.42 (m, 1H), 9.22 (d, *J* = 8.3 Hz, 1H), 8.57 (d, *J* = 9.0 Hz, 1H), 8.44 (dd, *J* = 8.3, 1.5 Hz, 1H), 8.30 (ddd, *J* = 8.8, 7.0, 1.5 Hz, 1H), 8.14 – 8.02 (m, 2H), 7.56 (d, *J* = 8.7 Hz, 1H), 6.57 (dd, *J* = 8.7, 2.4 Hz, 1H), 6.41 (d, *J* = 2.4 Hz, 1H), 5.11 (t, *J* = 9.3 Hz, 2H), 4.04 (t, *J* = 6.4 Hz, 2H), 1.78 (p, *J* = 6.7 Hz, 2H), 1.56 – 1.29 (m, 22H). ^{13}C NMR (75 MHz, CD_3OD) δ 195.6, 167.9, 165.4, 150.3, 149.0, 139.4, 137.3, 136.1, 132.2, 131.8, 131.4, 123.0, 119.7, 116.7,

109.3, 102.0, 69.6, 59.4, 31.14, 31.13, 30.6, 30.5, 30.4, 30.2, 30.1, 27.5, 27.0, 24.2. LRMS (ESI^+) *m/z* 462 $(M)^+$. HRMS (ESI^+) *m/z* 462.3010 ($C_{30}H_{40}NO_3$ requires 462.3008).

5.2. Biology

5.2.1. Test Organisms and culture media. Three strains of *Trypanosoma brucei* (bloodstream form, BSF) were used in this study: (1) Wild type strain *Trypanosoma brucei brucei* Lister 427 (427-WT) [35]; (2) A multi-drug resistant strain, B48, which was created from 427-WT after deletion of the TbAT1 drug transporter [36] followed by adaptation to increasing concentrations to pentamidine [19]; (3) A 427-WT-derived clone, *Tb*AOX, generated by transfecting the wild-type cells with the vector pHD1336 [37] containing the TAO gene, exactly as described for the expression of TbAT1 [38].

All *T. b. brucei* strains were used as bloodstream trypomastigotes, and cultured in standard HMI-9 medium, supplemented with 10% heat inactivated fetal bovine serum (FBS), 14 µL β-mercaptoethanol, and 3.0 g/L $NaHCO_3$ (pH 7.4). Parasites were cultured in vented flasks at 37 ºC in a 5% CO_2 atmosphere and were passaged every 3 days. Bloodstream forms of the *T. congolense* savannah-type strain IL3000 were cultured exactly as described by Coustou et al [39]; the strain was kindly provided by Theo Baltz (Université Victor Segalen Bordeaux 2, Bordeaux, France).

5.2.2. Drug susceptibility assays. The drug susceptibilities of bloodstream form trypanosomes *T. b. brucei* s427 and B48 were determined using the resazurin assay as previously described [40, 41], with slight modifications. The assays were performed in 96-well plates with of 2×10^4 cells/well for *T. brucei* and 5×10^4 cells/well for *T.*

congolense. Trypanosomes and test drugs were incubated for a period of 48 hours followed by the addition of 20 µL of Alamar Blue solution (125 mg/L resazurin sodium salt (Sigma-Aldrich) in phosphate buffered saline (PBS), followed by a further 24 h incubation. Four trypanocides were used as positive controls including: pentamidine, diminazene aceturate, salicylic hydroxamic acid (SHAM), and phenylarsine oxide (PAO) (all from Sigma-Aldrich). Fluorescence was measured using a FLUOstar Optima (BMG Labtech, Durham, NC, USA) at wavelengths of 544 nm for excitation, 590 for emission. EC_{50} values were calculated by non-linear regression using an equation for a sigmoidal dose-response curve with variable slope using Prism 5.0 (GraphPad Software Inc., San Diego, CA, USA). In vitro assays against *T. b. rhodesiense* STIB900 (compounds **15** and **16**) were performed as described previously [42].

5.2.3. Cytotoxicity assay using Human Embryonic Kidney (HEK)/ Human Foreskin Fibroblast (HFF) 293-T cells. Toxicity of drugs to mammalian cells was carried out in mammalian cell lines according to a method previously described [43], with slight modifications. Briefly, HEK or HFF cells were grown in a culture containing 500 mL Dulbecco's Modified Eagle's Medium (DMEM) (Sigma), 50 mL New-born Calf Serum (NBCS) (Gibco), 5 mL Penicillin/Streptomycin (Gibco) and 5 mL L-Glutamax (200 mM, Gibco). Mammalian cells were incubated at 37 ºC/5% CO_2 and were passaged when they reached 80-85% confluence in vented flasks. For the assay, cells were suspended at a density of 3×10^5 cells/mL, of which 100 µL was added to each well of a 96-well plate. The plate was incubated at 37 ºC/5% CO_2 for 24 h to allow cell adhesion. Serial drug dilutions were prepared in a separate sterile plate and 100 µL was transferred to the wells containing the cells; PAO was used as positive control. The plate was then incubated at 37 ºC/5% CO_2 for an additional period of 30 h followed by

the addition of 10 µL of resazurin solution (125 mg/L in PBS) and a final incubation at 37 ºC/5% CO_2 for 24 h. The plate was read in a FLUOstar OPTIMA fluorimeter at wavelengths 530 nm for excitation and 590 nm for emission. The data were analyzed using GraphPad Prism 5.0 to determine EC_{50} values. The selectivity index was calculated as EC_{50} (HEK) / EC_{50} (*Trypanosoma*).

5.2.4. Cloning and expression of physiologic Trypanosome Alternative Oxidase (ΔMTS-TAO). The pET SUMO expression system (Thermo Fisher Scientific) was used for the cloning of ΔMTS-TAO. After expression in the heme-deficient FN102 *E. coli*, the 11 kD SUMO moiety was cleaved off by the ULP-1 (Ubiquitin-like-specific protease 1) protease at the carboxyl terminal, producing the native TAO protein. TA cloning technology (Thermo Fisher Scientific) was used following the manufacturer's instructions. The technique depends on the ability of adenine (A) and thymine (T) on different DNA fragments to hybridize and become bonded in the presence of a ligase (the T4 ligase was used in this experiment). PCR products were amplified using Taq DNA polymerase, which adds an adenine to the 3' end of the PCR product. The PCR-amplified insert was then cloned into pET101-NHis_6SUMO, which is a linearized vector having a complementary 3' thymine (T) overhang.

5.2.5. Plasmid construction for recombinant TAO expression. A previous construct, the pTAO plasmid, containing the cDNA for TAO from *T. brucei brucei* TC221 as previously described by Nihei *et al.*,[44] was used as template for the amplification of TAO using 5'-AGCCGTAACCACGCATCGAGG-3' and 5'-CTTGTTGAAGCAGAGAATGAGCGC-3' as sense and antisense cloning primers, respectively, for full length TAO, while a 5'-AGCGACGCCAAAACACCTGTGTGGG-3' and 5'-

CTTGTTGAAGCAGAGAATGAGCGC-3' primer pair was used to amplify the gene segment without the MTS coding sequence (ΔMTS-TAO). Pfu Ultra II Fusion HS DNA polymerase (Stratagene) was used for the initial PCR amplifications followed by Taq DNA polymerase for addition of a 3'-A overhang. Following the manufacturer's procedure, gel-purified PCR product (TAO) containing the 3'-A overhang was inserted into pET-SUMO Expression plasmid vector (Thermo Fisher), and used for the chemical transformation of One Shot TOP10 *E. coli* cells (Thermo Fisher). Transformants colonies were then grown on 50 µg/mL kanamycin-supplemented Luria-Broth (LB) plates. Construct-positive clones were confirmed by colony PCR and were then selected for liquid culture in LB media for the amplification of vector construct. The TOYOBO MagExtractor kit (Osaka, Japan) was used for extraction of plasmids, which were subjected to further confirmation by sequence analysis. The $NHis_6$SUMO-tagged TAO was further subcloned into pET101 (Invitrogen), which contains a carbenicillin-resistance cassette. Following PCR and gene analyses, the correct construct was used to transform a heme-deficient *E. coli* FN102 host with a kanamycin resistance gene. The construct-positive colonies were selected under carbenicillin and kanamycin pressure, and selected for storage and expression experiments.

5.2.6. Preparation of inner membrane-rich fraction. Membrane samples were prepared as described by Kido *et al.* [14] with some modification. Briefly, glycerol stock of a $NHis_6$SUMO-TAO-pET101/FN102 colony was streaked onto a LB plate containing 100 µg/mL carbenicillin, 50 µg/mL kanamycin, and 50 µg/mL aminolevulinic acid (ALA) using a sterilized platinum rod spreader, which were then incubated at 37 °C overnight. From the many colonies that appeared, a single colony of the strain carrying the cDNA for *T. b. brucei* full-length or ΔMTS-TAO was used to

prepare a pre-culture in 100 mL of Luria Broth medium containing 10 mg carbenicillin, 5 mg kanamycin, and 5 mg ALA for 6 h at 37 °C in a shaking incubator set at 250 rpm. When the OD_{600} was 0.6, the pre-culture was transferred to centrifuge tubes and centrifuged at 8000 rpm for 3 minutes at 4 °C. The supernatant was discarded and the pellets were re-suspended with 20 mL of fresh culture media, and then centrifuged at 8000 rpm at 4 °C for 3 minutes. This wash process was repeated 2 more times to remove residual 5-aminolevulinic acid in the pellets. The pellets were resuspended and aerobically grown at 30 °C in a total volume of 6 L of S-medium containing, 0.2% (w/v) glucose, 50 g tryptone peptone, 25 casamino acid, 25 g yeast extract, 15 g KH_2PO_4, 52 g K_2HPO_4, 12.5 g $(NH_4)_2SO_4$, 3.25 g trisodium-citrate.$2H_2O$, 0.25 g $MgSO_4 \cdot 7H_2O$, 0.125 g $FeCl_3$, 0.125 g $FeSO_4 \cdot 7H_2O$, and 0.5 g carbenicillin, and 0.25 g kanamycin, dispensed into 10 flasks for maximum aeration. The initial OD_{600} of the culture was 0.02. Expression of soluble and active TAO was made possible by induction with 25 µM of the inducer, isopropyl β-D-thiogalactopyranoside (IPTG) when optical density at 600 nm (OD_{600}) reached 0.3; post-induction growth was for 12 h at 20 °C. The cells were harvested by centrifugation at 8000 rpm at 4 ºC for 5 minutes. Pellets were re-suspended in 50 mM Tris-HCl (pH 7.5) containing 0.1 mM phenylmethylsulfonyl fluoride (PMSF; Sigma-Aldrich), 40% (w/w) sucrose, and a protease inhibitor cocktail (Sigma). The cells were broken by a French press with pressure between 150 and 200 megapascal. Unbroken cells were removed by centrifugation at 8000×g for 10 min in a Beckman Optima L-90K ultracentrifuge (USA). Inner membranes of $NHis_6$SUMO-TAO-pET101/FN102 cells were fractionated in 40% sucrose by ultracentrifugation at 200,000×g for 1 h at 4 °C in a Beckman Optima L-90K (30 mL of 20% sucrose lysate was overlaid on 30 mL of 50 mM Tris-HCl pH 7.5 containing 40% (w/w) sucrose per ultracentrifuge tube). The buoyant rich

inner membranes were transferred to a fresh centrifugation tube, and a pellet of inner membranes was obtained by a further ultracentrifugation step at 200,000×g for 1 h (Beckman Optima L-90K, USA). The resulting brown-colored inner membrane pellet was re-suspended in 1.5 mL 50 mM Tris-HCl (pH 7.5) containing 20% (w/w) sucrose.

5.2.7. Membrane solubilisation. The inner membranes were resuspended with solubilisation buffer (6 mg/mL protein in 50 mM Tris–HCl, 14% (w/v) n-octyl-β-D-glucopyranoside (OG), 2 M $MgSO_4.7H_2O$, 20 % (v/v) glycerol, pH 7.3) at 4 °C (in the cold room). The membrane sample was maintained at 4 °C throughout the solubilization process. The solubilized membranes were ultracentrifuged at 42,000 rpm for 1 h at 4 °C. The total protein, quinol oxidase activities of the samples at various stages (i.e. before centrifugation, supernatant and pellet) were determined.

5.2.8. Purification of rTAO (fl and ΔMTS). Purified rTAO was obtained by means of a hybrid batch/column procedure using TALON metal affinity resin (Clontech, Mountain View, USA) containing Co^{2+} metal ion which has a strong affinity for the histidine tag on SUMO-TAO, according to the manufacturer's instructions and exactly as described previously for fl-rTAO [14].

5.2.9. Ubiquinol oxidase/TAO inhibition assay. The Ubiquinol oxidase activity of purified TAO was measured by recording the change in absorbance of ubiquinol-1, at 278 nm, on a double beam-dual wavelength spectrophotometer (Shimadzu UV-3000) over 2 minutes. Reactions were initiated by the addition of ubiquinol-1 (ε_{278}=15,000 M^{-1} cm^{-1}) after 2 min of pre-incubation at 25 °C in the presence of ΔMTS-TAO and 50 mM Tris-HCl (pH 7.4) in a total reaction volume of 1 mL. For TAO kinetics/inhibitor assays, the reaction was initiated by the addition of varying concentrations of ubiquinol-

1 after 2 min of pre-incubation at 25 °C in the presence of fixed amounts of ΔMTS-TAO and varying concentrations of the inhibitor, all in a 50 mM Tris-HCl (pH 7.4) buffer containing 0.05% (w/v) octaethylene glycol-monododecylether detergent.

The inhibitors were dissolved in DMSO to make a stock solution of 10 mM, which was stored at -20 ºC and used for the assay. The known TAO inhibitors ascofuranone and salicylhydroxamic acid (SHAM) were used as positive controls in the assay while an equal volume of DMSO was used as negative control. The DMSO had no effect on TAO activity (result not shown). Auto-oxidation of Ubiquinol-1 was determined as a control, using the same protocol but without TAO; none was observed. The purity of ΔMTS-TAO was tested in the presence of up to 1 mM ascofuranone (0, 0.01, 0.1, 1.0, 10.0 µM and 1 mM).

5.2.10. Chemicals. All chemicals were of analytical grade. Ubiquinone-1 and protease inhibitor cocktail were purchased from Sigma-Aldrich.; detergents were purchased from Dojindo Molecular Technologies Inc. (Kumamoto, Japan).

5.2.11. In vivo activity. *T. b. rhodesiense* (STIB900/luc) acute mouse model. The STIB900_luc acute mouse model mimics the first stage of the disease. *T. b. rhodesiense* parasites were genetically modified with pTb-AMluc construct [34] kindly provided by JM Kelly, containing red-shifted luciferase reporter gene (PpyRE9h). This genetically modified strain of *T. b. rhodesiense* transfected with a red-shifted luciferase gene allows monitoring of the parasitaemia by live imaging. Four female NMRI mice were used per experimental group. Heparinized blood from a donor mouse with approximately 5×10^6 /mL parasitaemia was suspended in PSG to obtain a trypanosome suspension of 1×10^5 /mL. Each mouse was inoculated i.p. with 10^4 bloodstream forms of STIB900/luc,

respectively. Compounds **15** and **16** were formulated in 100% DMSO and diluted 10-fold in distilled water. Compound treatment was initiated 3 days post-infection on four consecutive days in a volume of 0.1 mL/10 g (final concentration = 10 mg/kg). Three mice served as infected-untreated controls. They were not injected with the vehicle alone since we have established in our laboratory that these vehicles do not affect parasitaemia nor the mice (data not shown). Parasitaemia was monitored by whole-animal live imaging the day after the last treatment (day 7) and 3 days after treatment (day 10). The experiment was stopped on day 10 because parasitaemia relapse was detected in all the treated mice. For imaging, mice were inoculated i.p. with 200 µL D-luciferin (15 mg/mL in PBS) (Perkin Elmer), and 10 minutes later anaesthetised with 2.5% isofluorane. Light emission was recorded for 5 minutes using in vivo imaging systems (IVIS) (Perkin Elmer). Mice are considered cured if the bioluminescence signal at day 60 post-infection is not higher than the background level. In vivo efficacy studies in mice were conducted at the Swiss Tropical and Public Health Institute (Basel) (License number 2813) according to the rules and regulations for the protection of animal rights ("Tierschutzverordnung") of the Swiss "Bundesamt für Veterinärwesen". They were approved by the veterinary office of Canton Basel-Stadt, Switzerland.

5.3. Stability assessment of the inhibitors

5.3.1. Metabolic stability in serum. An adaptation of the protocol by L. Di *et al* was followed [25]. Stock solutions (2 mM in DMSO) of compounds **3**, **15**, **16**, **19**, **20**, **30** and ditialzem were prepared. For each test compound, 195 µL of a 50/50 (v/v) solution of sterile filtered mouse serum (Aldrich M6906) or horse serum (Sigma H-1270) in phosphate-buffered saline (PBS pH 7.4, isotonic) was dispensed in 6 Eppendorf tubes and the tubes were pre-incubated at 37 ºC for 15 min. The test compounds (5 µL of

stock solution) were added, and the sample was vortexed and incubated at 37 ºC at six different time points (0, 0.25, 0.5, 1, 2 and 24 h) with the serum. For each time point, the initiation of the reaction was staggered so all incubation times were terminated at the same time by addition of 600 µL of cold acetonitrile. For the time 0, the reaction was quenched with ice-cold acetonitrile right after mixing with serum. The tubes were vortexed and centrifuged at 4000 rpm for 15 min. The supernatant (600 µL) was transferred to 2 mL HPLC vials and 200 µL of 1.67 mM 2,5-dihydroxybenzoic acid (internal standard) in acetonitrile was added to each HPLC sample for LC–MS analysis. HPLC analysis was performed with a SunFire C18-2.1 µm column (4.6 mm × 50 mm); injection: 2 µL, flow rate: 0.35 mL/min, detection at 254 nm (ditialzem, **13**, **15** and **19**) and 316 nm (**3**, **16, 20** and **30**).

5.3.2. Microsomal stability. Microsomal stability of compounds **15** and **16** toward metabolism by cytochrome P450 (Phase-I metabolism) and Uridine diphosphate Glucuronosyl-Transfererase (UGT) (Phase-II metabolism) was studied in presence of NADPH and UDPGA, respectively. Incubation media (0.6 mL of final reaction volume) containing 0.8 mg/mL protein of human liver microsomes (HLM) (Gentest; Corning) or 1 mg/mL protein of human liver S9 fraction (Sigma-Aldrich) in 80 mM potassium phosphate buffer (pH 7.4) and **15**, **16** or diclofenac in 5 µM concentration were added with NADPH (1 mM), and incubated in a water bath at 37 ºC for 2 h. Alternatively, incubation media (0.6 mL of final reaction volume) containing human liver S9 mix fraction (1 mg/mL protein) in 80 mM potassium phosphate buffer (pH 7.4) with **15** or **16** in 5 µM concentration were added with UDPGA (2 mM), and incubated at 37 ºC for 2 h. Aliquots (100 µL) were withdrawn at 0, 15, 30, 60 and 120 min, added to 100 µL of acetonitrile, vortexed and centrifuged at 10000 rpm. An aliquot of supernatant (20 µL)

was analyzed by RP-HPLC (Agilent 1200 apparatus with a 1100 diode array detector (DAD) and a 1046A fluorescence detector) using a reversed phase 3.9 × 150 mm, 4 µm, Nova-pak C18 column (Waters, Milford, MA, USA) under the following chromatographic conditions: eluent A: 50 mM ammonium phosphate buffer (pH 3) and eluent B: 20 % A in acetonitrile. A linear gradient was used from 0 to 100% B in 8 min, and then 100% B for 10 min. Under these conditions **15** and **16** eluted at 12.8 and 10.5 min, respectively. **15** was determined at 230 and 265 nm, **16** at 237 nm and by fluorescence (237 nm, excitation and 400 nm, emission) and diclofenac at 280 nm. Assays were carried out at least in duplicate. Concentration of DMSO was <0.25%.

5.4. Molecular modeling of TAO-inhibitor complexes

The binding mode of TAO and SHAM derivatives was predicted by structural modelling using the TAO-AF2779-OH complex structure (PDB ID, 3AAV) [26] as a template. AF2779-OH is an ascofuranone (AF) derivative comprised of a substituted aromatic head and an isoprenoid tail. In the TAO-AF2779-OH structure, the inhibitor was bound tightly in the active site cavity with its aromatic head oriented towards the essential di-iron center, and its tail projecting out of the cavity [26]. For the modelling, the aromatic head of compounds **5**, **13**, **14**, **17**, **19**, **20**, and **28** was superposed on the head portion of the AF2779-OH using the coot program [45]. The model structure was subjected to 200 steps of energy minimization in order to avoid disallowed contacts, using the CNS software [46]. The models with the lowest energy scores (structurally most favorable binding pattern) were selected.

Supporting Information

Figures S1–S5. Table S1-S3. Method for SDS-PAGE of TAO. Preparation of Ubiquinol-1 (UQ1H2) from Ubiquinone-1 (UQ1). ^{1}H and ^{13}C NMR spectra for **14**, **15**, **16**, **28**, **30**, and **31**.

Author information

Corresponding Author

* Phone: +44 (0) 1413303753. E-mail: Harry.De-Koning@glasgow.ac.uk

* Phone: +34 912587490. E-mail: dardonville@iqm.csic.es

ORCID

Harry P. de Koning: 0000-0002-9963-1827

Christophe Dardonville: 0000-0001-5395-1932

Acknowledgements

This work was funded by the Spanish Ministerio de Economia y Competitividad (SAF2015-66690-R). This investigation also received financial support (ID No. B40103 to EOB) from TDR, the Special Programme for Research and Training in Tropical Diseases, co-sponsored by UNICEF, UNDP, the World Bank and WHO. G. U. Ebiloma was supported by a TET-fund studentship from the government of Nigeria and by a Mac Robertson Travel Scholarship from the College of Medical, Veterinary and Life Sciences of the University of Glasgow. We are indebted to Professor David Horn of the University of Dundee for making the *T. brucei aqp1-3*$^{-/-}$ strain available for this work. We thank Elena Yuste for technical assistance. EY is recipient of a “Garantia Juvenil” fellowship from Comunidad de Madrid (Fondo Social Europeo-Iniciativa de Empleo Juvenil).

Abbreviations used

AF, ascofuranone; ALA, aminolevulinic acid; AOX, alternative oxidase; BSF trypanosome, bloodstream form trypanosome; 2,4-DHBA, 2,4-dihydroxybenzoic acid; GK, glycerol kinase; G3P, glycerol 3-phosphate; HB, hydrogen bond; HAT, human African trypanosomiasis; HFF cells, human foreskin fibroblast cells; LC, lipophilic cation; MTS, mitochondrial targeting signal; PAO, phenylarsine oxide; RF, resistance factor; SHAM, salicylhydroxamic acid; SI, selectivity index; SPR, surface plasmon resonance; SUMO, small ubiquitin-related modifier; TAO, trypanosome alternative oxidase; TPP, triphenylphosphonium; SI, selectivity index.

References

[1] L. Young, T. Shiba, S. Harada, K. Kita, M.S. Albury, A.L. Moore, The alternative oxidases: Simple oxidoreductase proteins with complex functions, Biochem. Soc. Trans., 41 (2013) 1305-1311.

[2] M.P. Barrett, R.J. Burchmore, A. Stich, J.O. Lazzari, A.C. Frasch, J.J. Cazzulo, S. Krishna, The trypanosomiases, Lancet, 362 (2003) 1469-1480.

[3] F. Giordani, L.J. Morrison, T. Rowan, H.P. De Koning, M.P. Barrett, The animal trypanosomiases and their chemotherapy - a review, Parasitol. Int., 143 (2016) 1862-1889.

[4] K. Nakamura, S. Fujioka, S. Fukumoto, N. Inoue, K. Sakamoto, H. Hirata, Y. Kido, Y. Yabu, T. Suzuki, Y.-i. Watanabe, H. Saimoto, H. Akiyama, K. Kita, Trypanosome

alternative oxidase, a potential therapeutic target for sleeping sickness, is conserved among *Trypanosoma brucei* subspecies, Parasitol. Int., 59 (2010) 560-564.

[5] Y. Yabu, T. Suzuki, C. Nihei, N. Minagawa, T. Hosokawa, K. Nagai, K. Kita, N. Ohta, Chemotherapeutic efficacy of ascofuranone in *Trypanosoma vivax*-infected mice without glycerol, Parasitol. Int., 55 (2006) 39-43.

[6] Y. Yabu, A. Yoshida, T. Suzuki, C. Nihei, K. Kawai, N. Minagawa, T. Hosokawa, K. Nagai, K. Kita, N. Ohta, The efficacy of ascofuranone in a consecutive treatment on *Trypanosoma brucei brucei* in mice, Parasitol. Int., 52 (2003) 155-164.

[7] S.K. Menzies, L.B. Tulloch, G.J. Florence, T.K. Smith, The trypanosome alternative oxidase: a potential drug target?, Parasitology, (2016) 1-9.

[8] N. Minagawa, Y. Yabu, K. Kita, K. Nagai, N. Ohta, K. Meguro, S. Sakajo, A. Yoshimoto, An antibiotic, ascofuranone, specifically inhibits respiration and in vitro growth of long slender bloodstream forms of *Trypanosoma brucei brucei*, Mol. Biochem. Parasitol., 84 (1997) 271-280.

[9] A.B. Clarkson, Jr., E.J. Bienen, G. Pollakis, R.W. Grady, Respiration of bloodstream forms of the parasite *Trypanosoma brucei brucei* is dependent on a plant-like alternative oxidase, J. Biol. Chem., 264 (1989) 17770-17776.

[10] D.A. Evans, R.C. Brown, The inhibitory effects of aromatic hydroxamic acids on the cyanide-insensitive terminal oxidase of *Trypanosoma brucei*, Trans. R. Soc. Trop. Med. Hyg., 67 (1973) 258.

[11] P.T. Grant, J.R. Sargent, Properties of L-alpha-glycerophosphate oxidase and its role in the respiration of *Trypanosoma rhodesiense*, Biochem. J., 76 (1960) 229-237.

[12] F.J. Fueyo González, G.U. Ebiloma, C. Izquierdo García, V. Bruggeman, J.M. Sánchez Villamañán, A. Donachie, E.O. Balogun, D.K. Inaoka, T. Shiba, S. Harada, K. Kita, H.P. de Koning, C. Dardonville, Conjugates of 2,4-Dihydroxybenzoate and

Salicylhydroxamate and Lipocations Display Potent Anti-parasite Effects by Efficiently Targeting the *Trypanosoma brucei* and *Trypanosoma congolense* Mitochondrion, J. Med. Chem., 60 (2017) 1509-1522.

[13] Y. Kido, T. Shiba, D.K. Inaoka, K. Sakamoto, T. Nara, T. Aoki, T. Honma, A. Tanaka, M. Inoue, S. Matsuoka, A. Moore, S. Harada, K. Kita, Crystallization and preliminary crystallographic analysis of cyanide-insensitive alternative oxidase from *Trypanosoma brucei brucei*, Acta Cryst. F, 66 (2010) 275-278.

[14] Y. Kido, K. Sakamoto, K. Nakamura, M. Harada, T. Suzuki, Y. Yabu, H. Saimoto, F. Yamakura, D. Ohmori, A. Moore, S. Harada, K. Kita, Purification and kinetic characterization of recombinant alternative oxidase from *Trypanosoma brucei brucei*, Biochim. Biophys. Acta, Bioenerg., 1797 (2010) 443-450.

[15] V. Hamilton, U.K. Singha, J.T. Smith, E. Weems, M. Chaudhuri, Trypanosome Alternative Oxidase Possesses both an N-Terminal and Internal Mitochondrial Targeting Signal, Eukaryot. Cell, 13 (2014) 539-547.

[16] N.S. Curvey, S.E. Luderer, J.K. Walker, G.W. Gokel, Improved Syntheses of Benzyl Hydraphile Synthetic Cation-Conducting Channels, Synthesis, 46 (2014) 2771-2779.

[17] R. Ott, K. Chibale, S. Anderson, A. Chipeleme, M. Chaudhuri, A. Guerrah, N. Colowick, G.C. Hill, Novel inhibitors of the trypanosome alternative oxidase inhibit *Trypanosoma brucei brucei* growth and respiration, Acta Trop., 100 (2006) 172-184.

[18] F.H. Brohn, A.B. Clarkson, Jr., Quantitative effects of salycylhydroxamic acid and glycerol on *Trypanosoma brucei* glycolysis in vitro and in vivo, Acta Trop., 35 (1978) 23-33.

[19] D.J. Bridges, M.K. Gould, B. Nerima, P. Mäser, R.J.S. Burchmore, H.P. De Koning, Loss of the high-affinity pentamidine transporter is responsible for high levels

of cross-resistance between arsenical and diamidine drugs in african trypanosomes, Mol. Pharmacol., 71 (2007) 1098-1108.

[20] S.K. Vodnala, T. Lundbäck, E. Yeheskieli, B. Sjöberg, A.-L. Gustavsson, R. Svensson, G.C. Olivera, A.A. Eze, H.P. de Koning, L.G.J. Hammarström, M.E. Rottenberg, Structure–Activity Relationships of Synthetic Cordycepin Analogues as Experimental Therapeutics for African Trypanosomiasis, J. Med. Chem., 56 (2013) 9861-9873.

[21] J.C. Munday, A.A. Eze, N. Baker, L. Glover, C. Clucas, D. Aguinaga Andrés, M.J. Natto, I.A. Teka, J. McDonald, R.S. Lee, F.E. Graf, P. Ludin, R.J.S. Burchmore, C.M.R. Turner, A. Tait, A. MacLeod, P. Mäser, M.P. Barrett, D. Horn, H.P. De Koning, *Trypanosoma brucei* aquaglyceroporin 2 is a high-affinity transporter for pentamidine and melaminophenyl arsenic drugs and the main genetic determinant of resistance to these drugs, J Antimicrob. Chemother., 69 (2014) 651-663.

[22] L. Jeacock, N. Baker, N. Wiedemar, P. Mäser, D. Horn, Aquaglyceroporin-null trypanosomes display glycerol transport defects and respiratory-inhibitor sensitivity, PLOS Pathogens, 13 (2017) e1006307.

[23] Y. Yabu, N. Minagawa, K. Kita, K. Nagai, M. Honma, S. Sakajo, T. Koide, N. Ohta, A. Yoshimoto, Oral and intraperitoneal treatment of Trypanosoma brucei brucei with a combination of ascofuranone and glycerol in mice, Parasitol. Int., 47 (1998) 131-137.

[24] E.O. Balogun, D.K. Inaoka, T. Shiba, Y. Kido, T. Nara, T. Aoki, T. Honma, A. Tanaka, M. Inoue, S. Matsuoka, P.A. Michels, S. Harada, K. Kita, Biochemical characterization of highly active *Trypanosoma brucei gambiense* glycerol kinase, a promising drug target, J. Biochem., 154 (2013) 77-84.

[25] L. Di, E.H. Kerns, Y. Hong, H. Chen, Development and application of high throughput plasma stability assay for drug discovery, Int. J. Pharm., 297 (2005) 110-119.

[26] T. Shiba, Y. Kido, K. Sakamoto, D.K. Inaoka, C. Tsuge, R. Tatsumi, G. Takahashi, E.O. Balogun, T. Nara, T. Aoki, T. Honma, A. Tanaka, M. Inoue, S. Matsuoka, H. Saimoto, A.L. Moore, S. Harada, K. Kita, Structure of the trypanosome cyanide-insensitive alternative oxidase, Proc. Nat. Acad. Sci. , 110 (2013) 4580-4585.

[27] M.F. Bauer, S. Hofmann, W. Neupert, M. Brunner, Protein translocation into mitochondria: the role of TIM complexes, Trends Cell. Biol., 10 (2000) 25-31.

[28] W. Neupert, J.M. Herrmann, Translocation of proteins into mitochondria, Annual Rev. Biochem., 76 (2007) 723-749.

[29] M. Ohashi-Suzuki, Y. Yabu, S. Ohshima, K. Nakamura, Y. Kido, K. Sakamoto, K. Kita, N. Ohta, T. Suzuki, Differential kinetic activities of glycerol kinase among African trypanosome species: phylogenetic and therapeutic implications, J. Vet. Med. Sci., 73 (2011) 615-621.

[30] J.R. Haanstra, A. van Tuijl, P. Kessler, W. Reijnders, P.A. Michels, H.V. Westerhoff, M. Parsons, B.M. Bakker, Compartmentation prevents a lethal turbo-explosion of glycolysis in trypanosomes, Proc. Natl. Acad. Sci. U. S. A., 105 (2008) 17718-17723.

[31] A.H. Fairlamb, F.R. Opperdoes, P. Borst, New approach to screening drugs for activity against African trypanosomes, Nature, 265 (1977) 270-271.

[32] T. Suzuki, C.-I. Nihei, Y. Yabu, T. Hashimoto, M. Suzuki, A. Yoshida, K. Nagai, T. Hosokawa, N. Minagawa, S. Suzuki, K. Kita, N. Ohta, Molecular cloning and characterization of *Trypanosoma vivax* alternative oxidase (AOX) gene, a target of the trypanocide ascofuranone, Parasitol. Int., 53 (2004) 235-245.

[33] G. Pollakis, R.W. Grady, H.A. Dieck, A.B. Clarkson, Jr., Competition between inhibitors of the trypanosome alternative oxidase (TAO) and reduced coenzyme Q9, Biochem. Pharmacol., 50 (1995) 1207-1210.

[34] A.P. McLatchie, H. Burrell-Saward, E. Myburgh, M.D. Lewis, T.H. Ward, J.C. Mottram, S.L. Croft, J.M. Kelly, M.C. Taylor, Highly sensitive in vivo imaging of Trypanosoma brucei expressing "red-shifted" luciferase, PLoS Negl. Trop. Dis., 7 (2013) e2571.

[35] H.P. de Koning, A. MacLeod, M.P. Barrett, B. Cover, S.M. Jarvis, Further evidence for a link between melarsoprol resistance and P2 transporter function in African trypanosomes, Mol. Biochem. Parasitol., 106 (2000) 181-185.

[36] E. Matovu, M.L. Stewart, F. Geiser, R. Brun, P. Mäser, L.J.M. Wallace, R.J. Burchmore, J.C.K. Enyaru, M.P. Barrett, R. Kaminsky, T. Seebeck, H.P. De Koning, Mechanisms of arsenical and diamidine uptake and resistance in *Trypanosoma brucei*, Eukaryot. Cell, 2 (2003) 1003-1008.

[37] S. Biebinger, L.E. Wirtz, P. Lorenz, C. Clayton, Vectors for inducible expression of toxic gene products in bloodstream and procyclic *Trypanosoma brucei*, Mol. Biochem. Parasitol., 85 (1997) 99-112.

[38] J.C. Munday, K.E. Rojas Lopez, A.A. Eze, V. Delespaux, J. Van Den Abbeele, T. Rowan, M.P. Barrett, L.J. Morrison, H.P. de Koning, Functional expression of TcoAT1 reveals it to be a P1-type nucleoside transporter with no capacity for diminazene uptake, Int. J. Parasitol. Drugs Drug Resist., 3 (2013) 69-76.

[39] V. Coustou, F. Guegan, N. Plazolles, T. Baltz, Complete in vitro life cycle of *Trypanosoma congolense*: development of genetic tools, PLoS Negl. Trop. Dis., 4 (2010) e618.

[40] B. Rodenko, A.M. Van Der Burg, M.J. Wanner, M. Kaiser, R. Brun, M. Gould, H.P. De Koning, G.J. Koomen, 2,N^6-disubstituted adenosine analogs with antitrypanosomal and antimalarial activities, Antimicrob. Agents Chemother., 51 (2007) 3796-3802.

[41] R.M. Omar, J. Igoli, A.I. Gray, G.U. Ebiloma, C. Clements, J. Fearnley, R.A. Edrada Ebel, T. Zhang, H.P. De Koning, D.G. Watson, Chemical characterisation of Nigerian red propolis and its biological activity against *Trypanosoma Brucei*, Phytochem. Anal., 27 (2016) 107-115.

[42] C. Dardonville, C. Fernandez-Fernandez, S.L. Gibbons, N. Jagerovic, L. Nieto, G. Ryan, M. Kaiser, R. Brun, Antiprotozoal activity of 1-phenethyl-4-aminopiperidine derivatives, Antimicrob. Agents Chemother., 53 (2009) 3815-3821.

[43] B. Rodenko, M.J. Wanner, A.A.M. Alkhaldi, G.U. Ebiloma, R.L. Barnes, M. Kaiser, R. Brun, R. McCulloch, G.-J. Koomen, H.P. de Koning, Targeting the Parasite's DNA with Methyltriazenyl Purine Analogs Is a Safe, Selective, and Efficacious Antitrypanosomal Strategy, Antimicrob. Agents Chemother., 59 (2015) 6708-6716.

[44] C. Nihei, Y. Fukai, K. Kawai, A. Osanai, Y. Yabu, T. Suzuki, N. Ohta, N. Minagawa, K. Nagai, K. Kita, Purification of active recombinant trypanosome alternative oxidase, FEBS letters, 538 (2003) 35-40.

[45] P. Emsley, K. Cowtan, Coot: model-building tools for molecular graphics, Acta Cryst. D, 60 (2004) 2126-2132.

[46] A.T. Brunger, P.D. Adams, G.M. Clore, W.L. DeLano, P. Gros, R.W. Grosse-Kunstleve, J.S. Jiang, J. Kuszewski, M. Nilges, N.S. Pannu, R.J. Read, L.M. Rice, T. Simonson, G.L. Warren, Crystallography & NMR system: A new software suite for macromolecular structure determination, Acta Cryst. D, 54 (1998) 905-921.

Highlights

- The physiologically relevant ΔMTS-TAO was expressed and purified for the first time.
- Nanomolar range inhibitors of ΔMTS-TAO were discovered.
- The inhibitors displayed nanomolar range EC_{50} values against WT and drug-resistant strains of *T. brucei* and *T. congolense*.
- Compounds' metabolic stability in liver microsomes and mouse serum was studied.
- Compounds **15** and **16** showed in vivo activity against *T. b. rhodesiense*.